

Materials Degradation of Aircraft

by

© Sina Khakzad Rostami

A thesis submitted to the

School of Graduate Studies

In partial fulfillment of the requirements for the degree of

Master of Engineering

Faculty of Engineering & Applied Science

Memorial University of Newfoundland

May 2019

St. John's, Newfoundland

“Dedicated to my family for their unconditional love and affection”

ABSTRACT

One of the most critical area on which aviation industry research is still focused relates to the construction materials for airframe structure. There are certain requirements must be met by candidates to construct the airframes, which are basically determined by primary factors such as strength, weight, and reliability. Amongst these materials, aluminum alloys due to their unique characteristics are being widely used by aircrafts manufactures. The attractiveness of aluminum relies on its moderately low cost, high strength-to-weight ratio, ease of fabrication, good stiffness and fracture toughness. On the other hand, there, similar to other construction materials, are drawbacks associated with the use of aluminum alloys; susceptibility to damage by corrosion and fatigue. This study investigate the corrosion susceptibility of the bulk aluminum alloys found in airplane structure, 2000 (Al-Cu-Mg) and 7000 (Al-Zn-Mg-Cu) series, in different pH and temperatures. In addition, the corrosion protection efficiency of zinc-phosphate and epoxy resin as primer coatings are examined by electrochemical techniques.

ACKNOWLEDGEMENTS

I would like to express my sincere sense of gratitude and respect to my supervisor Professor John Shirokoff for his expert guidance and untiring support throughout my research at Memorial University of Newfoundland. Needless to say, without his encouragement and advice, this thesis might not have been completed successfully.

I would also like to thank Memorial University and Bombardier Inc. for funding and providing the facilities necessary to conduct my research and thesis work.

Table of Contents

Abstract	III
Acknowledgements.....	IV
Table of contents.....	V
List of Tables	VII
List of Figures	VIII
List of Symbols and Abbreviations	X
1. Introduction.....	1
1.1. Research Objectives	4
2. Literature Review.....	6
2.1. Aluminum Alloys	6
2.1.1. Aluminum Alloys Temper Designation System.....	13
2.2. Corrosion of Aluminum Alloys	14
2.2.1. Corrosion Environment.....	14
2.2.2. Corrosion of High Strength Aluminum Alloys	15
2.3. Aluminum Alloys Corrosion Prevention	20
2.3.1. Cladding of Aluminum	20
2.3.2. Coating of Aluminum Alloys	21
2.4. Related Studies.....	25

3. Experimental Setup.....	30
3.1. Material Selection and Preparation.....	30
3.2. Coating Preparation	34
3.3. Electrochemical Measurement.....	35
3.3.1. Electrochemical Impedance Spectroscopy	36
3.3.2. Polarization Resistance Technique	37
3.4. Experiment Series	38
4. Results and Discussion	39
4.1. Electrochemical Impedance Spectroscopy	39
4.1.1. EIS Tests on Bare and Coated Aluminum Alloy 2024-T3	42
4.1.2. EIS Tests on Bare and Coated Aluminum Alloy 7075-T6	35
4.2. Polarization Resistance Tests.....	41
4.2.1. Tafel Tests on Bare and Coated Aluminum Alloy 2024-T3	43
4.2.2. Tafel Tests on Bare and Coated Aluminum Alloy 7075-T6	44
5. Conclusions.....	60
6. Appendix	61
7. References	79

List of Tables

Table 1: Wrought aluminum alloys series	34
Table 2: Classification of wrought aluminum Alloys	37
Table 3: Strength ranges of wrought aluminum alloys	38
Table 4: Temper designation for aluminum alloys	40
Table 5: AA 2024 elemental composition	41
Table 6: AA 7075 elemental composition	42
Table 7: Seawater composition	53
Table 8: Experimental conditions	53

List of Figures

Figure 1: Coating components used in aerospace industry	24
Figure 2: A picture of a cut sheet to samples	32
Figure 3: A bare sample before and after mounting	33
Figure 4: A bare sample after application of nail polish	33
Figure 5: Coated sample by Zinc-Phosphate and Epoxy	35
Figure 6: Equivalent circuit used for EIS analysis	39
Figure 7: Bode plots of coated AA 2024 in different pH at 20 °C	43
Figure 8: Nyquist plots of coated AA 2024 in different pH at 20 °C	44
Figure 9: Bode plots of bare AA 2024 in different pH at 20 °C	45
Figure 10: Nyquist plots of bare AA 2024 in different pH at 20 °C	45
Figure 11: Bode plots of coated AA 2024 in pH 6 and pH 9.5 at 30 °C	46
Figure 12: Bode plot of coated AA 2024 in pH 7.9 at 30 °C	46
Figure 13: Nyquist plots of coated AA 2024 in pH 6 and pH 9.5 at 30 °C	47
Figure 14: Nyquist plot of coated AA 2024 in pH 7.9 at 30 °C	47
Figure 15: Bode plots of bare AA 2024 in pH 6 and pH 9.5 at 30 °C	48
Figure 16: Bode plot of bare AA 2024 in pH 7.9 at 30 °C	49

Figure 17: Nyquist plots of bare AA 2024 in pH 6 and pH 9.5 at 30 °C	49
Figure 18: Nyquist plot of bare AA 2024 in pH 7.9 at 30 °C	50
Figure 19: Bode plots of coated AA 2024 in pH 6 and pH 9.5 at 40 °C	51
Figure 20: Bode plot of coated AA 2024 in pH 7.9 at 40 °C	51
Figure 21: Nyquist plots of coated AA 2024 in pH 6 and pH 9.5 at 40 °C	52
Figure 22: Nyquist plot of coated AA 2024 in pH 7.9 at 40 °C	52
Figure 23: Bode plots of bare AA 2024 in pH 6 and pH 9.5 at 40 °C	53
Figure 24: Bode plot of bare AA 2024 in pH 7.9 at 40 °C	53
Figure 25: Nyquist plots of bare AA 2024 in pH 6 and pH 9.5 at 40 °C	54
Figure 26: Nyquist plot of bare AA 2024 in pH 7.9 at 40 °C	54
Figure 27: The corrosion rate of bare AA 2024 at different temperatures and pH.....	56
Figure 28: The corrosion rate of coated AA 2024 at different temperatures and pH.....	57
Figure 29: The corrosion rate of bare AA 7075 at different temperatures and pH	58
Figure 30: The corrosion rate of coated AA 7075 at different temperatures and pH.....	59

List of Abbreviations and Symbols

Abbreviations

AA: Aluminum Alloy

EIS: Electrochemical Impedance Spectroscopy

PR: Polarization Resistance

SEM: Scanning Electron Microscopy

CR: Corrosion rate

Cu: Copper

Mg: Magnesium

Zn: Zinc

CPE: Constant phase element

R: Resistance

Z: Impedance

Symbols

MPa: Mega Pascal

f: frequency

g: Gram

A: area

m³: cubic meter

mm/y: mili inches per year

Chapter 1

1. Introduction

Now, it is more than a century which the first powered aircraft was successfully built by Wright brothers in 1903. Since then, aircraft industry have seen an ever-going advancement in all aspects of their construction. One of the most critical area on which aviation industry research is still focused relates to the construction materials for airframe structure. There are certain requirements must be met by each material considered to construct the airframes, which are basically determined by primary factors such as strength, weight, and reliability [1]. The material must be strong enough to support all the complex state of loads applied during take-off, flying, and landing. Further, lightweight materials improve an airplane performance by letting it fly faster and further, and making commercial airplanes more economical by increasing the size and decreasing fuel consumption [2]. Moreover, the construction materials need to maintain a certain level of reliability in order to prevent any unexpected failure which could be fatal in aviation section.

There are different metallic and non-metallic materials which are used in airframe structures as a function of above mentioned initial requirements. Wood as the original material of choice for manufacture of early aircrafts structural components is no longer of use due to presence of other materials having higher strength-to-weight ratios for lightweight and corrosion resistant structures [3]. The main groups of construction metals

which are presently applied in aerospace structures includes aluminum alloys, titanium alloys, and steel alloys. After wood, aluminum has been the major material of airframe construction. Aluminum alloys have extensive use in fuselage, wing, and supporting structures of both commercial and military aircrafts. In addition, composites due to their high stiffness and strength, low weight, and excellent corrosion resistance have recently become popular in manufacture of modern aircrafts. At present, carbon-fiber composite is the most prevalent material for airframe construction along with aluminum alloys. Composites are both lighter and stronger than aluminum; although, they suffer high cost and low impact damage tolerance [4]. Using composite materials owing to their unique properties has decreased the role of aluminum to some extent. However, aluminum appears one of the critical structural materials in aerospace industry.

The attractiveness of aluminum relies on its moderately low cost, high strength-to-weight ratio, ease of fabrication, good stiffness and fracture toughness. On the other hand, there, similar to other construction materials, are drawbacks associated with the use of aluminum alloys; susceptibility to damage by corrosion and fatigue. Different properties of aluminum alloys are controlled by alloying elements composition and heat treatment such that their properties are designed for specific structural applications. For example, the alloy used for upper wing skins needs to support high bending loads whereas the one for lower wing skins must provide high fatigue resistance [4].

Amongst aluminum alloys, 2000 (Al-Cu-Mg) and 7000 (Al-Zn-Mg-Cu) series are the bulk aluminum found in airframe structures. Both series are heat treatable (precipitation-hardenable), achieving their strength through the precipitation of fine coherent precipitates

and dispersoids. Among 2000 alloy series, 2024-T3 is the most used in aerospace applications, taking advantage of cold-working followed by natural aging. Moderate yield strength, good fracture toughness, and good resistance to fatigue crack growth are considered as its advantages. However, it is susceptible to exfoliation corrosion. To overcome this issue, it is usually clad with a layer of high-purity aluminum providing galvanic protection of the core material against corrosion. 2024 has application in airframe where high damage tolerance is required such as lower wing skins and fuselage structure. Also, the most widely used conventional alloy among 7000 series, is 7075-T6, solution heat treated followed by artificially aging. Characterized as a high strength alloy, it is used in aircraft structures needing to carry high stresses such as upper wing skins, wing tension members and fuselage skins. Higher strength, however, decreases the corrosion resistance and makes it highly susceptible to stress corrosion cracking when used in thicker plates [2, 5].

Aluminum is considered as a passive metal such that a thin aluminum oxide film, chemically bound to the surface, is naturally formed preventing the substrate from more oxidation. This passivation behavior makes aluminum very resistant to general corrosion. The protective layer, however, becomes unstable and breaks down at specific points when exposed to extreme pH levels, leading to formation of localized corrosion [6 & 7]. Therefore, in order to avoid unexpected failures and high costs of unscheduled maintenance due to corrosion, aluminum needs to be protected effectively. A viable solution, as mentioned above, is cladding the alloys with high purity aluminum in order to take advantage of high corrosion resistance of pure aluminum along with mechanical properties

of high strength aluminum alloy located in the core [8, 9]. Furthermore, a coating system is employed as extra protection against both corrosion and extreme environment conditions. The coating system usually consists of three coating layers; a conversion coating, a primer, and the top coat [10]. The first layer is a very thin inorganic layer providing corrosion protection and improves adhesion to the primer. The second layer, the primer, has a similar function to the conversion coat, but is composed of a pigmented organic resin matrix. At last, the top coat, usually a polyurethane resin, is applied as the main barrier against environmental influences and providing decoration and camouflage. Hexavalent chromium, or chromate, appears as the best way to hinder corrosion of aluminum alloys such that conversion coating and primer layers are mostly formulated with compounds containing chromate. However, chromates and other chromium containing compounds has been shown to have carcinogenic effects [11]. Therefore, there have been many efforts to find a suitable replacement for chromate corrosion inhibiting compounds. As a result, Zinc Phosphate was found one the initial candidates. The present study goal is testing the performance of Zinc Phosphate, as a conversion coat, and epoxy resin, as a prime layer, applied on clad aluminum alloys 2024-T3 and 7075-T6 in natural seawater. It should be noted that there is no top-coat to be considered in this research.

1.1. Research Objectives

The funding for this research was made available through the purchase of Bombardier 415 “Superscooper” aircraft by the Government of Newfoundland and Labrador and the Industrial Regional Benefits Program.

The Bombardier 415 “Superscooper” is an amphibious water bomber that is used worldwide in firefighting operations. While fulfilling this roll, the Bombardier 415 is exposed to corrosion environments above and beyond those of regular aircraft. The “Superscooper” is routinely in intimate contact with marine environments while collecting fresh or salt water for firefighting operations and is capable of landing in bodies of water or unpaved runways when operating in remote locations.

This funding provided an opportunity to conduct corrosion research on aircraft materials used in the construction of the Bombardier 415 that are exposed to harsh marine environments and the coating systems designed to protect them from corrosion. Currently all of the high strength aluminum plate or sheet used in the construction of aircraft is protected from corrosion by a three-layer coating system. Conversion coating and primer layers formulated with compounds containing chromate show the best protection aluminum alloys. However, chromates and other chromium containing compounds has been shown to have carcinogenic effects [11]. The goal of present research is to investigate the performance of Zinc Phosphate, as a conversion coat, and epoxy resin, as a prime layer, as suitable replacement for chromate corrosion inhibiting compounds.

Chapter 2

2. Literature Review

2.1. Aluminum alloys

Aluminum has been playing an important role in aerospace industry for decades as it was the primary replacement of wood in airframe structure. Statistics show that aluminum accounts for 60–80% of the airframe weight in most modern airplanes and other aerospace vehicles. Despite of fading aluminum application as a result of growing composites use over last decade, aluminum will likely remain a critical structural material due to its unique features. The advantage of aluminum use returns to its characteristics such as moderate cost, ease of fabrication, high specific stiffness and specific strength, light weight, ductility, fracture toughness, fatigue resistance, and controllable properties by means of mechanical and heat treatments. Similar to any other construction material aluminum also suffers drawbacks including poor mechanical properties at high temperature (above 150 °C), susceptibility to exfoliation and stress corrosion cracking, low dissimilar corrosion resistance, and inconvenient weldability of its age-hardened alloys [4].

Aluminum alloys are generally divided in two main groups; cast compositions and wrought compositions. In terms of mechanical properties, wrought alloys are far more superior to casting ones, such that casting aluminum alloys may just be used in non-load-bearing parts on aircrafts. Each group is further classified based on their respond to heat treatment into

heat treatable and non-heat treatable alloys. The heat treatments include solution heat treatment, quenching, and precipitation hardening [4, 5]. Heat treatment is applied to change metallurgical structure (e.g. crystal structure, grain size, dislocation density, precipitates), to improve mechanical properties (e.g. yield strength, fatigue resistance, fracture toughness, to increase environmental durability (e.g. corrosion resistance, oxidation resistance) or to alter the internal residual stress state [4]. In addition, many other wrought alloys properties are developed through mechanical reduction coupled with various annealing processes, known as work hardening [5]. Wrought alloys are further recognized as non-age-hardenable and age-hardenable. The differentiation originates from the ability of the latter group to gain strength by precipitation hardening (age-hardening) when heat treated. Most of the alloys in the former group have a yield strength of below 300 MPa, making them not suitable for use in airframe structure. On the other hand, the yield strength of age-hardenable alloys ranges between 450 and 600 MPa making them suitable for use in a wide variety of structural and semi-structural parts on aircraft [4].

Aluminum alloys are also categorized into alloy series according to their chemical compositions. The International Alloy Designation System (IADS), as a widely recognized system in aerospace industry, categorizes aluminum alloys based on their chemical composition. There are generally eight series and all aluminum alloys are placed into one of them. The principal alloying elements determine the family in which the alloy is placed. These eight series and the main alloying element(s) for each family are given in Table 1. It should be noted that the 8000 series do not follow the same rule as others, and only contains those alloys that cannot be allocated to the other series. However, the main alloying

element in 8000 series is usually lithium. For wrought alloys, which are of our interest in this study, a four-digit system is employed to list all of wrought composition families [4].

Table 1. Wrought aluminum alloys series (Adrian P. Mouritz, 2012) [4]

Alloy series	Main alloying element(s)	
1000	Commercially pure Al (>99% Al)	Not age-hardenable
2000	Copper	Age-hardenable
3000	Manganese	Not age-hardenable
4000	Silicon	Age-hardenable (if magnesium present)
5000	Magnesium	Not age-hardenable
6000	Magnesium and silicon	Age-hardenable
7000	Zinc	Age-hardenable
8000	Other (including lithium)	Mostly age-hardenable

The wrought alloys series are briefly introduced as follow [5];

1xxx: Controlled unalloyed (pure) composition, with applications primarily in the electrical and chemical industries.

2xxx: Copper is the prime alloying element in these series of alloys, although other elements especially magnesium may be present. 2xxx series alloys with yield strengths as high as 455 MPa are generally used in aircraft where their high strength is valued.

3xxx: Manganese is the main alloying element here, used as general-purpose alloys for architectural applications and various products.

4xxx: Silicon is the major alloying element in these alloys, used in welding rods and brazing sheet.

5xxx: Magnesium is the principal alloying element in this family, has application in boat hulls, gangplanks, and other products exposed to marine environments.

6xxx: Magnesium and silicon are the key alloying elements, commonly used for architectural extrusions and automotive components.

7xxx: Zinc is the principal alloying element in these series; although, other elements such as copper, magnesium, chromium, and zirconium, may be specified. The 7xxx series with yield strengths ≥ 500 MPa possible, are the strongest aluminum alloys mainly used in aircraft structural components and other high-strength applications.

8xxx: Alloys characterizing miscellaneous compositions. The 8xxx series alloys may contain appreciable amounts of tin, lithium, and/or iron.

The different combinations of alloying elements, strengthening mechanisms, and strength ranges achievable for wrought aluminum alloys are shown in Table 2 and 3.

Table 2. Classification of wrought aluminum alloys based on strengthening mechanism [5]

Alloy system	Aluminum series
Work-hardenable alloys	
Pure Al	1xxx
Al-Mn	3xxx
Al-Si	4xxx
Al-Mg	5xxx
Al-Fe	8xxx
Al-Fe-Ni	8xxx
Precipitation-hardenable alloys	
Al-Cu	2xxx
Al-Cu-Mg	2xxx
Al-Cu-Li	2xxx
Al-Mg-Si	6xxx
Al-Zn	7xxx
Al-Zn-Mg	7xxx
Al-Zn-Mg-Cu	7xxx
Al-Li-Cu-Mg	8xxx

Table 3. Strength ranges of various wrought aluminum alloys [5]

Aluminum Association series	Type of alloy composition	Strengthening method	Tensile strength range	
			MPa	ksi
1xxx	Al	Cold work	70–175	10–25
2xxx	Al-Cu-Mg (1–2.5% Cu)	Heat treat	170–310	25–45
2xxx	Al-Cu-Mg-Si (3–6% Cu)	Heat treat	380–520	55–75
3xxx	Al-Mn-Mg	Cold work	140–280	20–40
4xxx	Al-Si	Cold work (some heat treat)	105–350	15–50
5xxx	Al-Mg (1–2.5% Mg)	Cold work	140–280	20–40
5xxx	Al-Mg-Mn (3–6% Mg)	Cold work	280–380	40–55
6xxx	Al-Mg-Si	Heat treat	150–380	22–55
7xxx	Al-Zn-Mg	Heat treat	380–520	55–75
7xxx	Al-Zn-Mg-Cu	Heat treat	520–620	75–90
8xxx	Al-Li-Cu-Mg	Heat treat	280–560	40–80

As it can be seen from Table 2, aluminum wrought alloys which are heat-treatable (precipitation-hardenable) include the 2xxx, 6xxx, 7xxx, and some of the 8xxx alloys. Further, since 2xxx and 7xxx series are the primary aluminum alloys used in airframe structure, and alloys of our interest in this study, the focus is put on those and are introduced in details below.

2xxx series: These alloys have copper as the main alloying element and usually magnesium as the secondary element. To obtain the best properties, they need to be solution heat treated. This results in mechanical properties equivalent and sometimes superior to those of low-carbon steels. Precipitation heat treatment may also be employed to further improvement of yield strength, which consequently leads to some loss of elongation [5].

Alloying elements play the key roles in developing the alloy properties. Cu, Mg, and Zn forms intermetallic precipitates (e.g. CuAl_2 , Al_2CuMg , ZnAl) through reaction with aluminum during heat treatment, resulting in increase of strength and fatigue resistance. In addition, Mn and Cr which are present in small amounts creates dispersoid particles (e.g. $\text{Al}_{20}\text{Cu}_2\text{Mn}_3$, $\text{Al}_{18}\text{Mg}_3\text{Cr}_2$), limiting grain growth and boosting yield strength through grain boundary hardening [4].

Similar to most of aluminum alloys, this family of aluminum alloys also suffer corrosion susceptibility, particularly intergranular corrosion. To overcome this problem these alloys are commonly produced in clad form to provide galvanic protection of the core alloy. The cladding layer usually are a high-purity aluminum, a magnesium-silicon alloy of the 6xxx series, or an alloy containing 1% Zn, making 2 to 5% of the total thickness on each side [5].

Many types of 2000 alloys have been developed, but only some of them have application in aircraft structures. Amongst them, Al 2024 (Al–4.4Cu–1.5Mg) is virtually the most common one used to manufacture of components such as stringers, longerons, spars, bulkheads, carry-throughs, stressed skins and trusses. 2000 series are basically present everywhere in the structure demanding high fatigue resistance and damage-tolerance. New generation of 2000 alloys are developed with superior properties to Al 2024. As an example, Al 2054 has 15–20% higher fracture toughness and two times higher fatigue resistance compared to Al 2024. Other 2000 series used in aircraft include Al 2018, 2025, 2048, 2117, and 2124. Minimizing impurities, specifically iron and silicon, has improved fracture toughness and resistance to fatigue crack initiation and crack growth [4].

7xxx series: In this family of aluminum alloys, zinc is the principal alloying element. It is, although, the addition of magnesium in small amount that make them heat-treatable alloys of moderate to very high strength. Other elements are usually added to improve the properties, some of which are copper, chromium, and scandium.

The high strength of these alloys after age-hardening comes from precipitates of CuAl_2 , Mg_2Al_3 , $\text{Al}_{32}(\text{Mg}, \text{Zn})_{49}$ [4, 5]. Having higher strength compared to 2xxx series, alloys of 7xxx family are used in highly stressed airframe structure components such as upper wing surfaces, spars, stringers, framework, pressure bulkheads and carry-through.

Higher strength 7xxx alloys show poor corrosion resistance and are mainly susceptible to stress corrosion cracking. Therefore, they are often utilized in a slightly over-aged temper to provide better combinations of strength, corrosion resistance, and fracture toughness. The most common alloy in 7xxx family used in aircraft is Al 7075. There are other 7xxx

alloys used in aircraft structures including Al 7049, 7050, 7079, 7090, 7091, 7178, and 7475. The Boeing 777 is typical of most modern aircraft in that it uses both conventional and new aluminum alloys [4].

2.1.1. Aluminum alloys temper designation system

The type of temper performed on aluminum alloys is specified by a system of numbers and letters known as the temper designation system. Basic temper designations are composed of single capital letters while major subdivisions are shown using numbers. The temper designation comes after alloy designation, separated by a hyphen. For example Al 2024-T6 indicates that the alloy has been tempered to the T6 condition involving solution treatment followed by artificial ageing. Table 4 shows the letters and numbers commonly used in the designation system of aluminum alloys [4].

Table 4. Temper designations for aluminum alloys [4]

F	As-fabricated (eg. hot-worked, forged, cast, etc.)
O	Annealed (wrought products only)
H	Cold-worked (strain hardened) H1x – cold-worked only (x refers to amount of cold working and strengthening) H2x – cold-worked and partially annealed H3x – cold-worked and stabilised at a low temperature to prevent age-hardening
W	Solution-treated
T	Age-hardened T1 – cooled from fabrication temperature and naturally aged T2 – cooled from fabrication temperature, cold-worked and naturally aged T3 – solution treated, cold-worked and naturally aged T4 – solution treated and naturally aged T5 – cooled from fabrication temperature and artificially aged T6 – solution-treated and artificially aged T7 – solution-treated and stabilised by over-ageing T8 – solution-treated, cold-worked and artificially aged T9 – solution-treated, artificially aged and cold-worked T10 – cooled from fabrication temperature, cold-worked and artificially aged

2.2. Corrosion of Aluminum Alloys

2.2.1. Corrosion Environment

Aircrafts structures are exposed to a variety of environments during their operation life. This means a wide range of corrosive substances and conditions threaten their integrity. For example, air pollutants such as sulfur dioxide and nitrogen dioxide in urban and industrial atmospheres cause corrosion by contribution to acid rain formation. In marine atmosphere salt and humidity are the major causes of corrosion. Also the difference in high and low altitudes temperature where airplanes operates can sometimes reach to more than 100 degree Celsius, resulting in cyclic temperature and stresses that ease corrosion fatigue

process. In addition to cyclic temperatures, each single flight involves taking-off and landing of the airplane, resulting in cyclic stresses and subsequent stress corrosion cracking and corrosion fatigue. Condensation of vapor due to pressurized cabin also provides a suitable environment for crevice corrosion formation. The other common corrosion in airframe structures includes contact of dissimilar metals, inducing galvanic corrosion if not protected sufficiently [12].

2.2.2. Corrosion of High Strength Aluminum Alloys

Aluminum appears among the passive metals, such that a passive layer (aluminum oxide) is formed when exposed to oxygen, preventing further corrosion attack. This layer with an excellent adhesion to the substrate, protects aluminum against most of chemical attacks. It is also electricity insulator and shows self-healing properties when damaged. Having passivation behavior, rate of aluminum corrosion decreases in a short time, and will be protected mostly against general corrosion in environment such as atmosphere and seawater [9].

As mentioned, aluminum resist corrosion very well owing to its passivation behavior. However, some aluminum alloys, specifically the ones having copper as the main alloying element, are at risk of localized corrosion. These localized corrosion can be categorized into two groups. One group, including pitting, crevice corrosion, and filiform corrosion are caused by local aggressive environments which break the oxide layer. The other group consisting of inter-granular corrosion and environmentally assisted cracking, take place generally because of metallurgical composition and thermal history of the alloys [9].

Corrosion in form of pits is the most prevalent corrosion found on aluminum alloys. Pitting corrosion involves two stages; pit initiation and pit growth. An initial pit can form where there is a mechanical damage of the passive film, particles of a second phase, localized stresses in form of dislocations, and non-homogeneous environments that may dissolve the passive layer. Presence of chloride ions highly accelerate pitting corrosion by easing the breaking of the oxide layer. After pit initiation, the pH of the electrolyte inside the pit decreases due to formation of hydrogen ions, which causes pit growth [13].

Crevice corrosion occurs when volumes of stagnant solution are trapped in the gap or crevice between two metals, or a metal and a non-metal surfaces. A difference in concentration of oxygen between inside and outside of crevice sets up an electrochemical concentration cell. Oxygen content and pH inside the crevice are lower than outside, while chlorine ions are higher. Once a crevice formed, the progress mechanism is similar to pit growth in pitting corrosion. The major factors influencing crevice corrosion are crevice geometry, material structure and composition, and environmental variables [14, 15].

Filiform or under-film corrosion take place under coatings in form of threadlike filaments, filled with corrosion products. This type of corrosion is a serious problem on coated aluminum alloys in humid atmosphere. Filiform corrosion starts in defects in the coating and progresses in presence of aggressive ions (chloride, sulphate...), oxygen and sufficient relative humidity. The filament consists of a head and a tail, the head acting as an electrochemical cell. In case of aluminum, it has been shown that the head contained an acidic salt layer of aluminum chloride and its hydrolysis products, while the tail was filled with carbonate containing aluminum hydroxide [16, 17, 18, 19].

Inter-granular corrosion is a form of localized corrosion which attacks along the grain boundaries. The corrosion is induced due to micro-segregation of impurities or alloys specific phases precipitated on grain boundaries. As there is an electrode potential difference between the grain boundary and the grain itself, a galvanic cell forms when an electrolyte exists [20, 21].

In aluminum alloys with copper as a major alloying element, copper-rich second phase particles (Al_2Cu) precipitate in grain boundaries during cooling process, resulting in copper depletion from region in the immediate vicinity. Subsequently, as the adjacent region to the grain boundaries, due to copper depletion, are more electronegative than the alloys grain, a galvanic cell forms. This galvanic cell between cathodic copper-rich region and anodic copper-depleted region causes corrosion at grain boundaries. In aluminum alloys whose major alloying element is magnesium, magnesium rich second phase particles (Mg_2Al_3) form at grain boundaries leading to formation of the galvanic cell.

Heat treatments of aluminum alloys play the key role in control of abundance and distribution of second phase particles so do in their sensitivity to inter-granular corrosion. For example, in the alloys with copper content over-aging tempers lead to precipitation of second phase particles within the alloy grains, which in turn mitigates the potential difference between the grains and the regions adjacent to the grain boundaries. However, over-aging tempers reduce the alloy strength of up to 20% [22]. Also, in alloys containing magnesium, avoiding elevated temperatures for extended periods of time provides protection against inter-granular corrosion. This protection is due to retardation of Mg_2Al_3 particles from forming a continuous path along the grain boundary. Similar to pitting

corrosion, the progress of inter-granular corrosion is generally limited by oxygen depletion at the final depth of the corroded grain boundaries. Once this depth is attained, the inter-granular corrosion would spread laterally over surface of the affected aluminum alloy.

Environmental cracking refers to a corrosion cracking that is resulted from stress corrosion cracking (SCC), corrosion fatigue, and hydrogen embrittlement. Although each of these three can cause a premature failure of the structure by their own, there is a possibility of working alongside each other. Stresses causing environmental cracking include residual cold work, welding, thermal treatment, or applied loads during service and, to be effective, must be tensile [21, 23].

Hydrogen embrittlement occurs due to absorption of hydrogen by material which leads to a drastic reduction of ductility and load bearing capacity and consequent cracking and failure below the yield stress of material. Hydrogen embrittlement mechanism is not fully understood and presents one the most difficult problems. Hydrogen can be absorbed during the process of manufacturing, or be a by-product of general corrosion [21, 23].

Corrosion fatigue as it name suggests is caused by combined effects of cyclic stresses and corrosive environments. The cyclic stresses are below the yield stress of the material and it is believed to crack the oxide passive layer and accelerate the corrosion. A simultaneous exposure to a corrosive environment lead to the failure in much lower stresses and shorter time periods compared to non-corrosive environment. Interestingly, in corrosion fatigue, there is no fatigue limit load as there is in pure mechanical fatigue. The fatigue induced fracture appears brittle and the cracks are most often trans-granular. The corrosive environment assists a faster crack growth and/or crack growth at a lower tension level

compared with in dry air. In presence of an even relatively mild corrosive atmospheres fatigue strength of aluminum structures can be reduced drastically, down to 75 to 25 percent of the fatigue strength in dry air. Corrosion fatigue in aluminum is characterized by an “oyster shell” fracture surface formed from numerous plastic deformations or crack “jumps” caused by the combined effect of a corrosive environment and cyclic loading [13, 21, 23].

Stress corrosion cracking (SCC) is the cracking caused by the combination of tensile stresses and a corrosive environment. The impact of SCC on a material is usually placed somewhere between dry cracking and the fatigue threshold of that material. The tensile stresses required for SCC are either in the form of externally applied stresses or in the form of residual stresses [21].

SCC mainly affects aluminum alloys that are susceptible to inter-granular corrosion, the ones, as it was explained before, that second phase intermetallic particles formed during their heat treatment precipitate on the grain boundaries. Reasonably, heat treatments reducing susceptibility to inter-granular corrosion in aluminum alloys will also reduce the susceptibility to SCC. However, an optimal heat treatment protecting against the both forms of the corrosions is rarely the same. SCC of aluminum alloys is mostly observed in environments with relatively high humidity aggravated by the presence of halides, most commonly chloride, coupled with static stresses. Interestingly, SCC is induced by tensile stresses much lower than the yield strength of the affected material. The mechanism of stress corrosion cracking can be explained either by anodic dissolution in presence of a sustained tensile stress or assuming hydrogen embrittlement at grain boundaries coupled

with a sustained tensile stress [24]. Environment pH has a direct effect on SCC propagation, as increases at acidic pH values and decreases with increasing ph. It should be noted that thin aluminum products such as sheets are not susceptible to SCC, and also Alclad aluminum products are generally immune to SCC. Further, stretching of thicker aluminum products such as plates results in relieving internal stresses and will subsequently increase their resistance to SCC [25].

2.3. Aluminum Alloys Corrosion Prevention

2.3.1. Cladding of Aluminum

Aluminum is considered as a passive metal such that a thin aluminum oxide film chemically bound to the surface is naturally formed when exposed to oxygen that prevents the substrate metal from more oxidation. This passivation behavior makes aluminum very resistant to general corrosion. The protective layer, however, becomes unstable and breaks down at specific points when exposed to extreme pH levels, leading to formation of localized corrosion [6, 7].

In aerospace industry with zero tolerance for corrosion due to safety concerns, reliance on corrosion protection of the aluminum oxide layer seems impossible. Application of just protective coatings to the alloys appears also insufficient as any damage or defects will end up to localized corrosion initiation.

In 1927, Alcoa Corporation developed Alclad aluminum sheet and plate products to be the first commercially viable solution to this problem. In a hot rolling process two thin sheets of pure aluminum are rolled on a core of high strength aluminum alloy, forming a

metallurgically bonded composite sheet. The idea was to obtain both the excellent corrosion resistance of high-purity aluminum and the desirable mechanical properties of high strength 2000 alloys all in one product. After performing corrosion experiments, interestingly, the unprotected edges of the aluminum alloy were observed also not affected by corrosion. It was then concluded that the pure aluminum layer in addition to be a corrosion resistant barrier also provided cathodic protection to the high strength aluminum alloy core [8].

Amongst aluminum alloys, 2000 (Al-Cu-Mg) and 7000 (Al-Zn-Mg-Cu) series are the bulk aluminum found in airframe structures. These alloys are however susceptible to localized corrosion. Since alclad discovery, Al 1050A alloy and Al 7072 alloy are generally used for cladding 2000 series alloys and 7000 series alloys respectively. In aerospace industry, the cladding layers are applied to both sides of the sheets or plates, making up to of 5% of the total sheet or plate thickness per side [22].

2.3.2. Aluminum Alloys Coatings

Reaching to a viable solution to protect against corrosion, demands a mature understanding of the fundamental aspects of the material degradation. In general, a metal corrosion happens when five requirements are met. An active corrosion site includes an anode, cathode, continuous electrical contact between the anode and cathode, continuous electrolyte, and a cathodic reactant such as O_2 , H_2O , or H_2 . Further, the galvanic coupling increases the corrosion rate greatly. In this case, aluminum alloys 2024, and 7075 have the anodic (Al elements) and cathodic (Cu inclusions) sites in constant electrical contact.

Therefore, the remaining necessary conditions to form galvanic cell are contact with water, and with O_2 or H_2 for corrosion to occur. Reasonably, the only way to prevent galvanic cell formation is to block the metal contact with water and cathodic reactants [11].

With respect to the above discussion, an effective approach to prevent aluminum corrosion is using a coating system. This fact necessitates aerospace industry to invest on coatings to protect the aircraft fleet. The coatings offer improved adhesion, airframe structural integrity protection, visual aesthetics and other specific features related to observability.

A classic airframe coating system usually consists of three individual coating layers. Figure 1 illustrate a schematic of different coating components used in aerospace industry. The first layer, conversion coating, with a thickness of 10-60 nm offers corrosion protection to some extent and improves the adhesion of the primer to the substrate. This layer is considered as a product of substrate pretreatment that contains passivating inhibitors such as chromates. These inhibitors are reduced at the active corrosion sites such as inclusions, grain boundaries, and pits, to form unsolvable oxides. Subsequently, these oxides precipitate on the sites and block the contact between the metal and electrolyte and oxygen. As a result of limiting permeability of water and cathodic reactants, corrosion rate decreases [11]. For high strength aluminum alloys, like Al 2024 and Al 7075, chromate conversion coating (CCC) appears as the most effective surface pretreatment [11, 26]. The chromate coating system provide the aluminum surface with a steady protection and repair because of its unique inhibitive power. However, due to its carcinogenic effects, it is necessary to replace it by other non-hazardous inhibitors [26].

The second layer, primer, assumed as the main corrosion protector has a similar function to the first layer but made of a pigmented organic resin matrix. The primer thickness of interest on airframe is 25 micro meter due to weight limitations; although its thickness can vary from 5 to 200 micro meter. The primer is generally made of epoxy resin containing chromate and non-chromate pigments. In order to get an efficient protection, passivating inhibitors are often combined with a barrier coating. In a similar manner to corrosion inhibitors, the barrier coatings hinder the corrosion by restraining the cathodic reaction. This is done through blocking the contact of the electrolyte and oxygen to the substrate and limiting the electrons transportation to the metal surface [11]. From the inhibitors inclusion point of view, a desired protection is provided as long as the inhibitors concentration is higher than a minimum value (critical concentration) required for corrosion stop-off. This value need to be maintained to assure the protection over the years of the vehicle operation, particularly in points where are not easily accessible for maintenance [26].

The final layer, topcoat, is usually formulated using a white colored polyurethane resin with a thickness of 50 to 200 nm. Topcoat acts as the principal protection against environmental degradation and allows decoration of the aircraft [11]. To name a few, Synthetic Enamel, Polyurethane, and Acrylic urethane are the well-known topcoats used for airframes painting. Among them, the most frequent used topcoat is polyurethane. Having fairly high abrasion-, stain-, chemical-, and UV ray resistant properties put it on the top of the choice list in aviation industry [27].

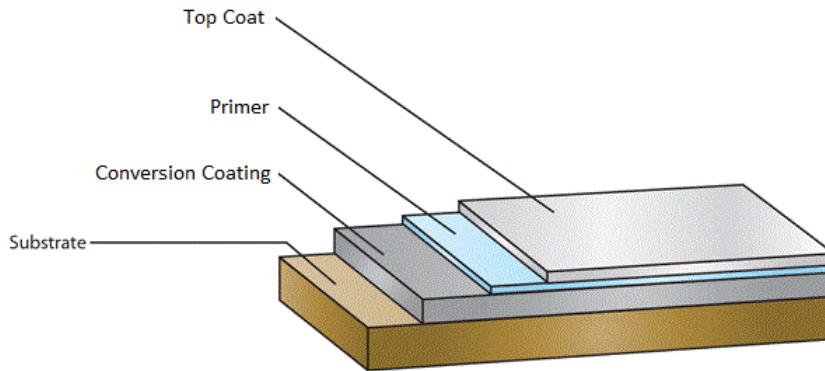


Figure 1. Coating components used in aerospace industry

The attractiveness of chromates relies on their powerful oxidizing features, solubility in water, the passive nature of their reduction products, cost effectiveness, and ease of application. The solubility of Cr^{6+} ions in water result in their delivery to the active corrosion sites, then reducing to Cr^{3+} and passivating the area [11, 28]. Research to find the replacements for chromate as active inhibitors reveals that the topmost candidates are cerium compounds, molybdates, vanadates and phosphates. Precipitation of cerium hydroxide ($\text{Ce}(\text{OH})_3$) at local regions of high pH is believed to be the mechanism controlling cathodic reaction [29]. Molybdate, similar to chromates, have good oxidizing power and stable reduction products. They also form a passive layer in order for corrosion protection; although, their effectiveness is limited by the size and solubility of the oxide MoO_2 species [30]. Zinc phosphates as the initial candidates, protects aluminum alloys against corrosion by formation of a $\text{Zn}_3(\text{PO}_4)_2 \times 4\text{H}_2\text{O}$ film with no toxic effects [31]. Phosphoric acid, zinc dihydrogen phosphate, fluoride and an oxidation accelerator are the elements of which bath composition is made. Further, electrochemical tests have revealed

that calcium strontium zinc phosphorsilicate offered the highest protection on aluminum 2024-T3 under damaged conditions among ten phosphate containing compounds [32]. It is worthy to note that this ranking was based on experiments on damaged (an 800 pm diameter hole) chromate conversion coated Al-2024-T3, such that chromate affects the inhibiting properties [11].

2.4. Related Research

In recent years, many research have been extensively done to find an alternative to chromate-based protective coatings for aluminum alloys, due to its carcinogenic effects. However, chromate conversion coatings (CCC) are still known as the best corrosion protection on aluminum alloys. In this section some of the most recent research performed to investigate coatings providing corrosion protection on aluminum alloys comparable to chromate-based coatings are reviewed.

In an effort to find an alternative for chromate conversion coating, Hongwei et al. [33] studied the corrosion protection properties of phytic acid conversion coatings on 2024-T3 aluminum alloy. They prepared the film under acidic conditions with various pH values and performed scanning electron microscopy (SEM), Energy-dispersive X-ray spectroscopy (EDS), ATR-FTIR and electrochemical techniques to observe and analyze the results. They claimed that the conversion coatings obtained by immersing the alloy in phytic acid solutions at pH from 3 to 5.5 provide excellent corrosion resistance. Also, ATR-FTIR results confirm that the film is formed by deposition of reaction products between Al^{3+} and phosphate groups in phytic acid molecules.

In a similar work by Honwei et al. [30] the corrosion protection of AA 2024-T3 in 0.05 M NaCl by cerium cinnamate was investigated. They claimed that polarization measurements demonstrated that cerium cinnamate appears fairly effective for suppressing anodic process of the alloy corrosion during the initial 72 h of immersion. The protection mechanism during the immersion test was reported to be composed of stages: the deposition of cerium cinnamate, and then hydrolysis of cerium ions forming a cerium oxide/hydroxide, prevailing over the foregoing deposition. They also illustrated the inhibition effect of cerium cinnamate on the early corrosion attack from the second phase particles by X-ray photoelectron spectroscopy and electron-probe microanalysis.

Rodriguez et al. [35] investigated performance of a molybdate conversion coating (MoCC) to protect aluminum alloy AA2024-T6. They determined the corrosion resistance of the coating by monitoring the open circuit potential (OCP) of the coated sample and evaluating polarization behavior. The authors claimed that a comparison between these results to an un-coated sample of aluminum alloy 2024-T6 showed that the layer formed was not just a superficial layer but a protection to the underlying aluminum alloy. They reported that the coating ennobled the corrosion potential of AA2024-T6 and protected the underlying aluminum alloy via anodic inhibition. According to authors, SEM revealed the surface morphology to be made of a mud cracked pattern that is similar to what would be seen on a sample coated with a chromium conversion coating.

José Ignacio et al. [36] conducted a research on AA2024-T3 in an accelerated corrosion environment, and examined the influence of different surface pre-treatments, the presence of a silane layer as pre-coating treatment, and the effect of phosphonic acids combined with

the silane layer on the corrosion protection and adhesion to the aluminum alloy. They stated that a good combination of a metal pre-treatment on AA2014-T3, followed by a deposition of a thin layer of an organic–inorganic silane coating and a layer of epoxy coatings, provide protection against corrosion in high concentrations of NaCl solution. They also reported that high roughness and application of a pre-coating film before the organic coating were essential for a good protection and resistance to blistering appearance in the surface of the alloy.

In a research by Wen Zhu et al. [37] a Titanium/Zirconium/Vanadium conversion coating (TZVCC) was coated on AA6063 and studied as a replacement to CCC. Scanning electron microscopy (SEM), X-ray photoelectron spectroscopy (XPS), atomic force microscope (AFM) and contact angle measuring device were used to characterize both the TZVCC treated alloy and CCC treated alloy. Also, the corrosion resistance of the TZVCC coated and CCC coated AA6063 evaluated using electrochemical measurements and neutral salt spray tests. According to the authors, the surface roughness and surface free energy of the alloy were significantly increased after TZVCC treatment, and the corrosion resistance of TZVCC was superior to that of CCC on AA6063. Further, pull-off tests and electrochemical impedance spectroscopy (EIS) were performed to evaluate the effects of the TZVCC and CCC on the adhesion properties and anti-corrosion performance of epoxy coating as a second layer coating. They reported that the dry, wet and recovery adhesive strengths of the epoxy coating on TZVCC coated samples were so close to those of epoxy coating on CCC treated ones. The authors even claimed that the samples coated with epoxy

and TZVCC showed a better corrosion resistance than samples coated with epoxy and CCC.

Liangliang Li et al. [38] investigated the formation, structure and corrosion performance of a commercial Zr/Ti-based conversion coating (Bonderite M-NT 5200, Henkel Corp.) on AA2024-T3. The specimens were coated by immersion in a coating bath made of a mixture of fluorozirconic and fluorotitanic acids (ca. 1:3) at a pH of 2–3. The coating was characterized by scanning electron microscopy, transmission electron microscopy, energy dispersive X-ray analysis and Auger electron spectroscopy (depth profiling) for coating morphology and chemical composition. Also, the authors employed electrochemical techniques to evaluate the corrosion inhibition performance of the coating. The coating included an outer layer of hydrated ZrO_2/TiO_2 on the order of 30 nm thick (in vacuo) and an interfacial region of approximately 60–90 nm between the coating and the alloy surface. In the coating, the Ti levels were twice greater than the Zr levels, consistent with the concentration differences in the coating bath. The authors reported that the no significant corrosion protection was observed under the test conditions based on similarities in the OCP, anodic and cathodic polarization curves, and polarization resistances measured for the uncoated and coated samples in a naturally-aerated 0.5 M Na_2SO_4 .

Chang-Sheng Liang et al. [39] conducted a research to develop a surface treatment method for aluminum foil using molybdate-based coating. After coating the aluminum foil samples with molybdate-based solution, they employed scanning electron microscopy, energy dispersive spectroscopy, and X-ray photoelectric spectroscopy to investigate the microstructure and composition of the resulting conversion coatings. The study shows that

the molybdate-based conversion coating was mostly made of MoO_3 , $(\text{MoO}_3)_x$, $(\text{P}_2\text{O}_5)_y$, and $\text{Al}_2(\text{MoO}_4)_3$ compounds. Moreover, corrosion protection efficiency of the coated samples was estimated using electrochemical impedance spectroscopy and potentiodynamic polarization. The authors reported that molybdate-based conversion coatings provided a noticeable corrosion protection. Also, they stated that the sample treated at $40\text{ }^\circ\text{C}$ exhibited the best corrosion resistance.

Chapter 3

3. Experimental Setup

The objective of performing the experiments in this study is finding the efficiency of zinc-phosphate as a conversion coating, and epoxy resin as a primer for improving corrosion resistance of aluminum alloys 2024 and 7075 commonly used in aircraft industry. Therefore, renowned electrochemical experiments have been employed for evaluation of the coatings applied on the metals. It is worthy to mention that although in aircraft industry three layers of coatings are normally applied, in this study only first two layers have been tested and the top coat has not been applied and considered.

3.1. Material Selection and Preparation

Clad aluminum alloys 2024-T3 and 7075-T6 were selected for corrosion test due to their extensive use in aircrafts. The metals were purchased online from Kaisar Aluminum Company in form of square sheets of 12×12 inches with a thickness of 0.16 inches (4.06 mm). The aluminum alloys compositions used in the experiments are shown in table 5 and table 6.

Table 5. Kaiser AA 2024 elemental composition

AA 2024											Others	
Weight %	Si	Fe	Cu	Mn	Mg	Cr	Zn	Ti	V	Zr	Each	Total
Min	0	0	3.8	0.3	1.2	0	0	0	0	0		
Max	0.5	0.5	4.9	0.9	1.8	0.1	0.25	0.15	0.05	0.05	0.05	0.15
Cladding Layer												
Min	0	0	0	0	0	0	0	0	0	0		
Max	0.25	0.3	0.1	0.05	0.05	0.03	0.05	0.03	0.03	0.03	0.03	0.09

Table 6. Kaiser AA 7075 elemental composition

AA 7075											Others	
Weight %	Si	Fe	Cu	Mn	Mg	Cr	Zn	Ti	V	Zr	Each	Total
Min	0	0	1.2	0	2.1	0.18	5.1	0	0	0		
Max	0.4	0.5	2	0.3	2.9	0.28	6.1	0.2	0.05	0.05	0.05	0.15
Cladding Layer												
Min	0	0	0	0	0	0	0.8	0	0	0		
Max	0.3	0.4	0.1	0.1	0.1	0.05	1.3	0.05	0.05	0.05	0.05	0.15

The sheets were then cut into the square specimens with a surface area of 1×1 inches by a water jet machine. Figure 2 shows the cut samples still attached to the sheet. Then, the sample edges were carefully polished using silicon-carbide sand papers 320 to remove the sharp edges.



Figure 2. A picture of a cut sheet to samples using water jet machine

Afterward, each sample was separately mounted, such that just top surface of the sample was left in exposure of the experiments. Figure 3 shows a bare sample before and after mounting. The reasons for mounting the samples were ease of handling and cleaning, preventing galvanic coupling on edges between cladding layers and the core alloy, and convenience of coating. This was followed by cleaning the exposed surfaces of the samples using methanol and distilled water. The cleaned samples, then, were dried by an air gun and remained in a desiccator for 24 hours. After the rest time, the surface of the sample where the perimeter of the metal meets the mounting material were fully covered by nail polish. This was done in order to get more accurate results by ceasing the contribution of the edges, place of stress concentration, to the test. Figure 4 shows a bare sample after application of nail polish to the edges.



Figure 3. A bare sample before mounting (Left). The same sample after mounting (Right)

As the nail polish covers some areas adjacent to the edges, the exposed surface area is no longer one square inch. This necessitates a careful measurement of the surface area as it would be an input for further electrochemical measurements. To do so, each nail-polished sample was taken picture, and the effective surface area was determined using ImageJ, an open platform for scientific image processing. Later, a small hole drilled and tapped to the side of each cylinder-shaped mounting to provide electrical connection to the metal through a screw for electrochemical measurements.

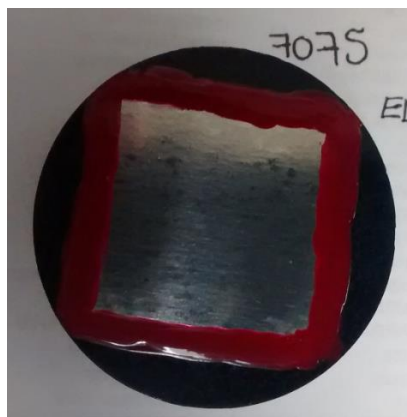


Figure 4. A bare sample after application of nail polish

3.2. Coating Preparation

Aerosol kits of zinc-phosphate primer as corrosion conversion coating and gallon kits of two component epoxy primer were purchased online from Aircraft Spruce Canada website. According to manufacture, Products Techniques Inc. (PTI) these primers “have been formulated specifically to inhibit corrosion, inhibit degradation, resist harmful chemicals and promote adhesion between the substrate and top coat, as they can be applied to nearly any substrate used in the construction of aircraft”.

After preparation of the materials as explained above, first, zinc-phosphate was applied on the samples. In a fume hood, the primer was perpendicularly sprayed on each sample from a point of 10 inches far from the metal surface continuously for 5 seconds. After spraying, the coated specimens were moved to a clean drawer and left for 48 hours to become dry.

Next step, included application of epoxy primer, which was done by means of immersion. After mixing the epoxy primer and its hardener in a container with a ratio of 1:1, each sample surface was immersed and left into the mixture for 60 seconds. This followed by drying the samples in atmosphere as they were placed in a clean drawer for 48 hours. Figure 5 shows coated samples as described.

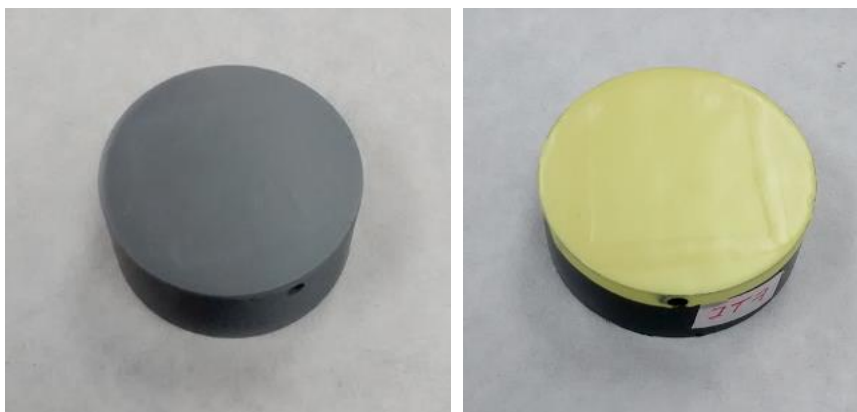


Figure 5. A coated sample with zinc-phosphate (Left). A sample coated with epoxy (Right)

3.3. Electrochemical Measurements

All experiments were conducted in a multi-port glass cell with a three-electrode setup at atmospheric pressure. A graphite rod was used as the counter electrode (CE), and saturated silver/ silver chloride (Ag/AgCl) was used as the reference electrode (RE). In order to investigate the electrochemical characteristics of the coating on the metal substrate, both coated and un-coated specimens subjected to corrosion environment were used as working electrodes (WE). In order to simulate real situation of corrosion environment, natural sea water was selected as electrolyte in the corrosion cell. Natural sea water was simply collected from Atlantic Ocean. The composition of the sea water is listed in table 7.

An Ivium Compactstat Potentiostat monitoring system and a Gamry 1010E potentiostat\galvanostat (<1% accuracy) were used to perform electrochemical corrosion measurements. Electrochemical impedance spectroscopy (EIS), and Polarization

Resistance techniques (Tafel plot) were employed to investigate the electrochemical characteristics of the coating and corrosion rate of the metal.

Table 7. Seawater composition

Specification	Concentration (ppm)
Sodium (Na ⁺)	1,078
Magnesium (Mg ²⁺)	1,284
Calcium (Ca ²⁺)	412
Potassium (K ⁺)	399
Chloride (Cl ⁻)	19,353
Sulfate (SO ₄ ⁻²)	2,712
Bicarbonate (HCO ₃ ⁻)	126
Other ions	114
Total salinity	35,181

3.3.1. Electrochemical Impedance Spectroscopy

Electrochemical Impedance Spectroscopy (EIS), also called AC Impedance or Impedance Spectroscopy is a powerful technique in corrosion and solid-state laboratories for characterization of electrochemical systems. The attraction of EIS lies on its ability to distinguish the dielectric and electric properties of individual components under investigation. EIS is considered as a non-destructive technique providing time-dependent quantitative data about the electrode and complex interfaces under study. Basically, electrochemical impedance method includes measuring the response of an electrode to a sinusoidal potential perturbation at different frequencies.

In this study, electrochemical impedance spectra were recorded at open circuit potential, in frequency range of 100 kHz to 10 mHz using an AC potential amplitude of 10 mV. The fitting of EIS data was performed in Ivium and Gamry Echem Analyst software.

3.3.2. Polarization Resistance Technique

Polarization resistance techniques have widespread application in laboratory corrosion testing, providing useful information regarding the corrosion mechanisms, corrosion rate and susceptibility to corrosion in designated environments. Polarization is defined as deviation of the electrochemical potential equilibrium by means of an electric current passing through the galvanic cell. Both the cathode and the anode can be polarized that are referred to as cathodic polarization and anodic polarization respectively. Resistance polarization is one type of polarization in which potential drop occurs by either the high resistivity of the electrolyte surrounding the electrode or an insulation effect of the film on the electrode surface formed by the reaction products.

Polarization resistance is defined by the following equation:

$$R_p = \frac{\Delta E}{\Delta i} \Delta E \rightarrow 0 \quad (1)$$

Where, ΔE is a variation of the applied potential around the corrosion potential and, Δi is the resulting polarization current.

Thus, polarization resistance is the ratio of the applied potential and the resulting current response. This "resistance" is inversely related to the uniform corrosion rate. Testing

polarization resistance is a useful technique that enables the estimation of a corrosion rate under steady-state conditions using Tafel slopes on the potentiodynamic scan. It is also used to describe the method of measuring corrosion rates using this slope.

In this study, the applied potential range for the potentiodynamic polarization measurements was from -0.250 V to $+0.250$ V with a scanning rate of 0.1 mV/s.

3.4. Experiment Series

Three sets of two types of electrochemical experiments have been done on the both alloys under study, in bare and coated conditions. Each single experiment has been conducted in three different hydrogen ion concentration (pH 6, pH 7.9, and pH 9.5), and three different temperatures (20, 30, and 40 degree Celsius). Also, to avoid errors and find the best results, each experiment has been repeated at least three times. Table 8 shows the experimental conditions.

Table 8. Experimental conditions

Test Series No.	Alloy Type	Test Type	Coat Type	Temp °C	pH
1	2024-T3 / 7075-T6	EIS/Tafel	Coated/Bare	20	6
					7.9
					9.5
2	2024-T3 / 7075-T6	EIS/Tafel	Coated/Bare	30	6
					7.9
					9.5
3	2024-T3 / 7075-T6	EIS/Tafel	Coated/Bare	40	6
					7.9
					9.5

Chapter 4

4. Results and Discussion

4.1. Electrochemical Impedance Spectroscopy

After performing EIS tests, Bode and Nyquist plots were obtained for analysis and interpretation of the data. To figure out the behavior of the corroding system, Equivalent Circuits (EC) are employed to fit on the obtained data. Each element used in EC should correspond to a physical structure in the corroding system, and a circuit element cannot be used merely to reach a better fit of the EC model to data. Dissimilar spectra shapes require individual equivalent circuits for analysis. The equivalent circuit used to fit on the data in this research is shown in figure 6. Every single circuit element describes a part of the corroding cell that is in contact with an electrolyte. In Figure 6, the equivalent circuit is overlaid on a schematic of a coated metal substrate.

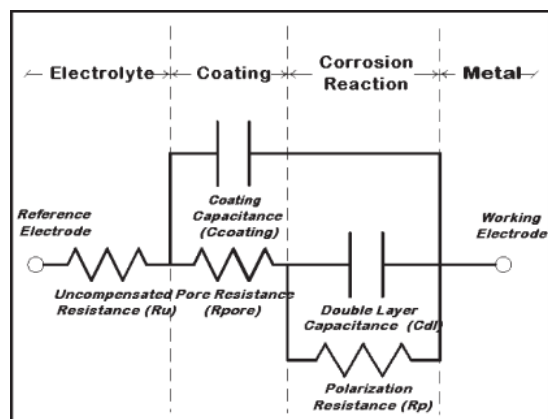


Figure 6. Equivalent circuit used for EIS analysis [40]

Uncompensated Resistance (RU): The resistance of the electrolyte between the working electrode and reference electrode. For studies of organic coatings, the electrolyte is very conductive, so Ru is usually very low (1-50 ohms) and can be ignored.

Coating Capacitance: Organic coating, acting as a capacitance, is another parameter to measure during coating failure. As most coatings are relatively thick, the coating capacitance tends to be rather low—in the range of 1 nF/cm². The physical and chemical properties of the coating that affect the capacitance are:

$$C_{\text{coating}} = (\epsilon) (\epsilon_0) (A) / t \quad (2)$$

where ϵ is the dielectric constant of the coating, ϵ_0 is 8.85×10^{-14} Farads/cm, A is the area (cm²), and t is the thickness (cm).

The capacitance is related to the magnitude of the impedance ($|Z|$) by

$$|Z| = 1 / (2 \pi f C_{\text{coating}}) \quad (3)$$

here f is the frequency of the applied AC voltage.

Pore Resistance: The micropores existing in the coating are represented as resistance of the coating. This resistance changes as electrolyte penetrates into the micropores of the coating during exposure. Upon immersion, the Pore Resistance can be very high ($>10^{10}$ ohm) and usually decreases with time of exposure to the electrolyte. However, R_{pore} can increase after long exposure times. This increase is commonly attributed to the blockage of the pores by corrosion products of the metal substrate [40].

Polarization Resistance (RP): This resistance describes the corrosion rate of the metal substrate beneath the coating. Since polarization resistance is inversely proportional to the corrosion rate, a metal corrosion rate in the absence of a coating can be determined from this parameter. A typical Polarization Resistance for a bare metal is 5000 ohm-cm². It should be noted that RP must be normalized as it is electrode area dependent [40].

Double Layer Capacitance (C_{dl}): In addition to the coating, there is another “structural” feature of the corroding cell that gives rise to a capacitance. There are charges on the metal electrode and the electrolyte that are separated by the metal electrolyte interface. Since this interface is commonly known as the “double layer” in electrochemical theory, the capacitance is called the Double Layer Capacitance. The value of C_{dl} is much higher than C_{coating}, usually in the range of 10–40 μF/cm². A scratch or holiday that exposes only 0.005% of the total sample area to the electrolyte has the same capacitance (20 μF * 0.005%) as the entire intact area of the coating (1 nF). A coating that is adhering strongly to the metal surface does not allow metal-electrolyte contact, so C_{dl} can sometimes be related to delamination of the coating. C_{dl} must be normalized because it is electrode area dependent [40].

In equivalent circuits initially two circuit elements dominate the impedance, the Coating Capacitance and the Pore Resistance. An undamaged coating with good barrier properties has a capacitance about 1 nF/cm². From equation (3), the impedance of 1 cm² of this coating at 1 Hz is about 10⁹ ohms and increases at lower frequencies. The Pore Resistance of this coating is exceedingly high (>10¹² ohm), so that the sample behaves as

a near-perfect capacitor. The impedance is high because there is no low impedance path through the sample. Needless to say, a coating that is under attack by an electrolyte, the values of the circuit elements will change (sometimes dramatically) as attack proceeds, which leads to changes in the EIS response [40].

4.1.1. EIS tests on coated and uncoated clad AA 2024-T3

Figure 7 and 8 show Bode plots and Nyquist plots of epoxy-coated clad AA 2024-T3 tested in temperature of 20 °C at three different pH respectively. Interestingly, the behavior of the corroding cell in varying hydrogen concentration at room temperature remains almost identical, as can be seen from both Bode and Nyquist diagrams. The Nyquist plot for each case displays a single capacitive loop, represented by a depressed semicircle, indicating presence of one time constant. This time constant semicircle is originated from one RC unit in the circuit, which in this case consists of a parallel connection of the coating capacitor (CPE_{coat}) and the coating resistance (R_{coat}). The diameters of the semicircles (the largest arc at natural pH of seawater, and the smallest one at low pH) are hydrogen concentration dependent. This may indicate that the electrochemical behaviors corresponding to the arcs are controlled by the hydrogen-reduction charge-transfer process.

The impedance of a capacitor can be expressed as

$$Z_{capacitor} = Z_{re} + j Z_{im} \quad (4)$$

$$= 0 + j [-1 / (2 \pi f C)]$$

$$= j [-1 / (2 \pi f C)]$$

Since the impedance of a capacitor is inversely proportional to the frequency ($1/f$, or f^{-1}), the Bode magnitude plot for a capacitor appears a straight line with a slope of -1 . Also, the Bode phase plot is a horizontal line at -90° as the phase shift of a capacitor is always 90° [40].

Accordingly, as seen in the Bode plots, nearly perfect capacitor characteristics appears for the all three pH in range of high frequency to almost 100 Hz. As the frequency decreases, the graphs approach to a resistive behavior. Finally at low frequency range, less than 100 mHz, the Bode plots show nearly pure resistive characteristics, such that the impedance magnitude plot becomes a horizontal line and phase angle closes to zero.

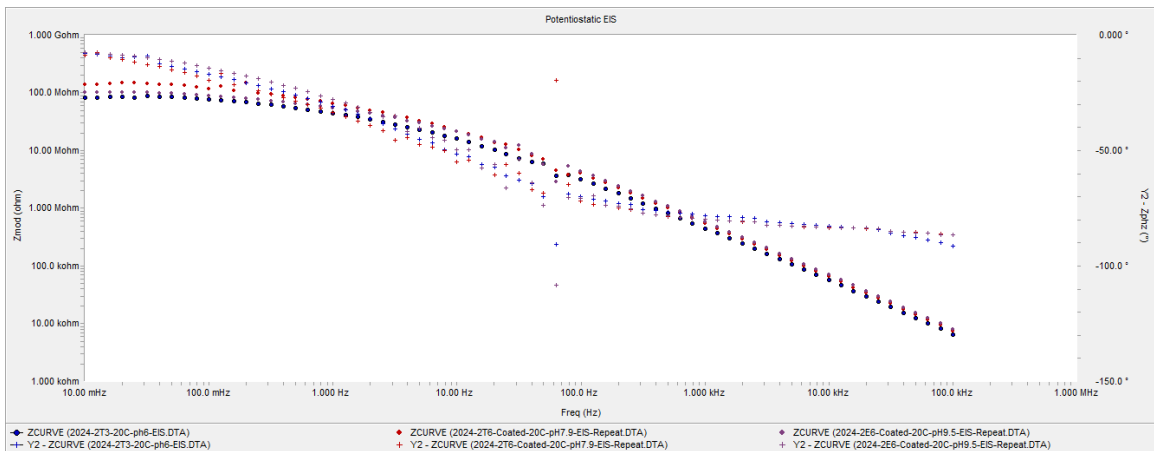


Figure 7. Bode plots of coated AA 2024 in different pH at 20 °C

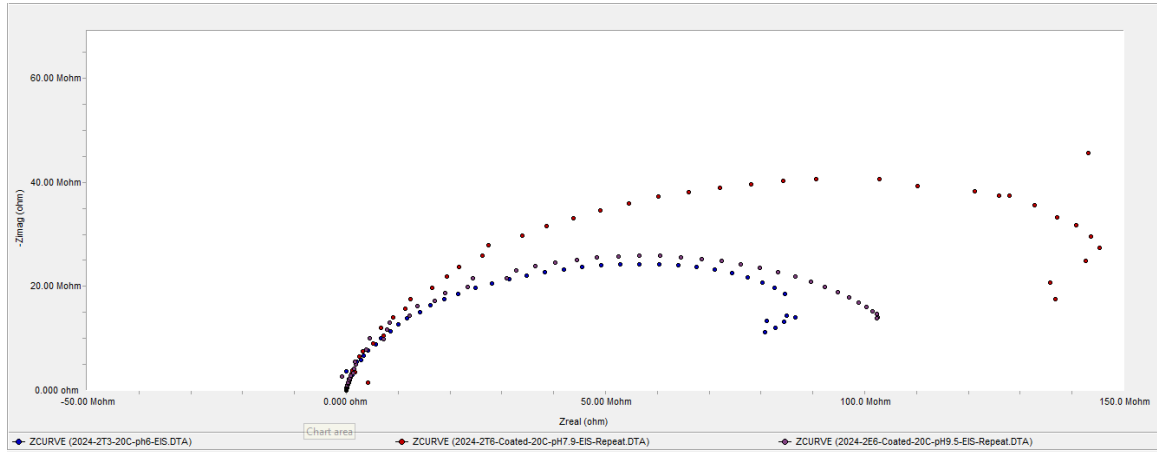


Figure 8. Nyquist plots of coated AA 2024 in different pH at 20 °C

Figure 9 and 10 show Bode plots and Nyquist plots of bare AA 2024-T3 tested in temperature of 20 °C at three different pH respectively. As it can be seen from the Nyquist plots, the behaviour of the corroding system in the different pH are not similar. At the lower pH of 6, although plot is noisy, a conductive behaviour at low frequency is easily observed. Conductive behaviour at low frequency can be related to the adsorption of some species on the metal surface. At higher pH of 9, a capacitive semi-circle followed by a depressed semi-circle in low frequency is noted. The capacitive loop at the high frequency is related to the break down of the aluminium oxide layer. Also, the depressed second loop can be related to the charge transfer resistance and the double layer capacitance.

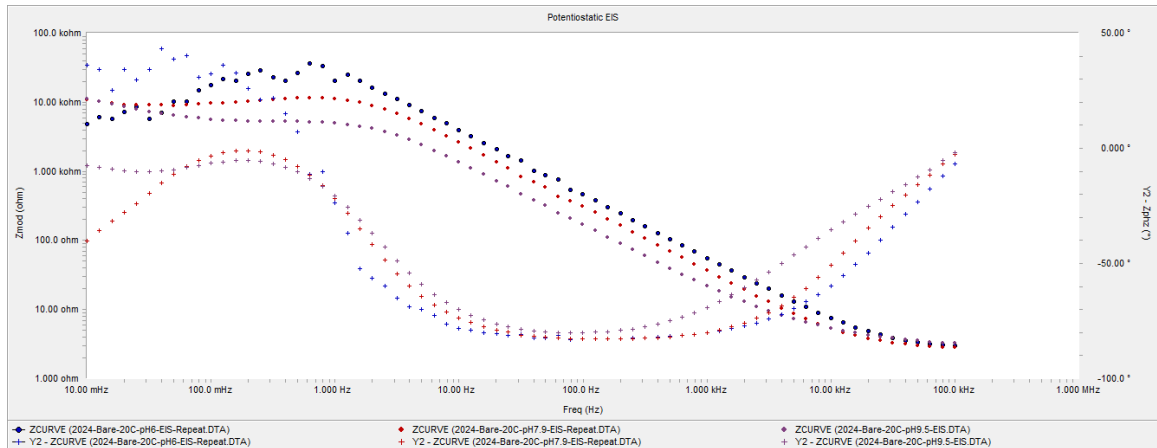


Figure 9. Bode plots of bare AA 2024 in different pH at 20 °C

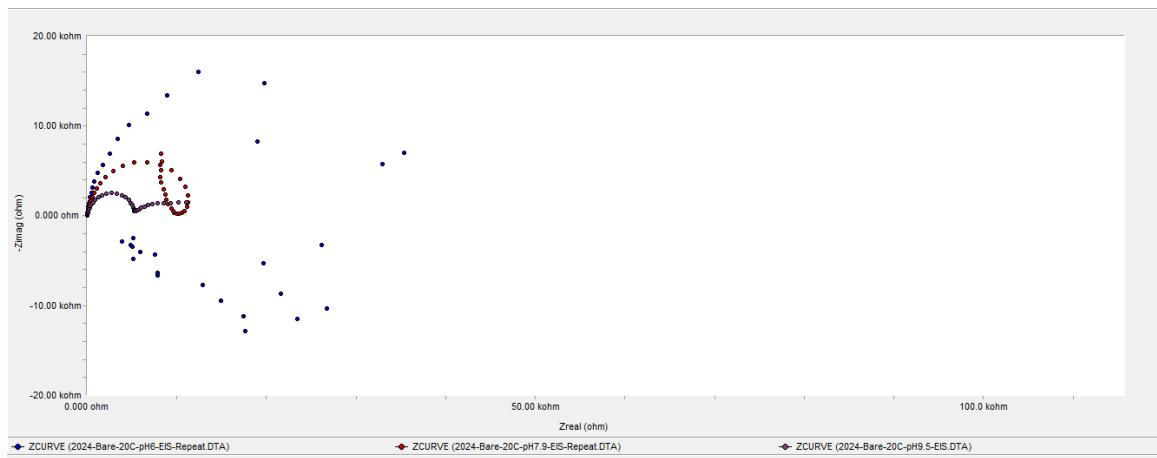


Figure 10. Nyquist plots of bare AA 2024 in different pH at 20 °C

Figure 11 to 14 show Bode plots and Nyquist plots of coated AA 2024-T3 tested in temperature of 30 °C for the varying pH. At 30 °C, the cell shows almost identical behavior for the varying pH. Also, both the Bode and Nyquist plots shapes are fairly similar to those of at 20 °C for coated samples. For all cases in Bode plot, a capacitive behavior is observed in high frequency followed by a resistive behavior in low frequency. It should be noted that the plot does not go sufficiently high in frequency to measure the solution resistance.

In fact, the solution resistance is not a property of the coating and related to the test solution and the test cell geometry. Therefore, it is not considered a problem in EIS measurement and not very interesting [Gamry, organic coat part 1].

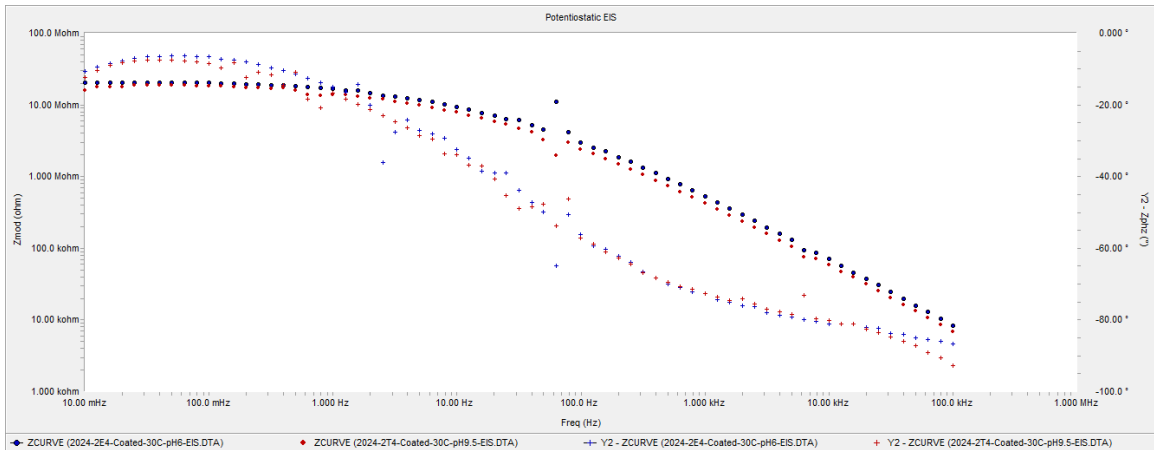


Figure 11. Bode plots of coated AA 2024 in pH 6 and pH 9.5 at 30 °C

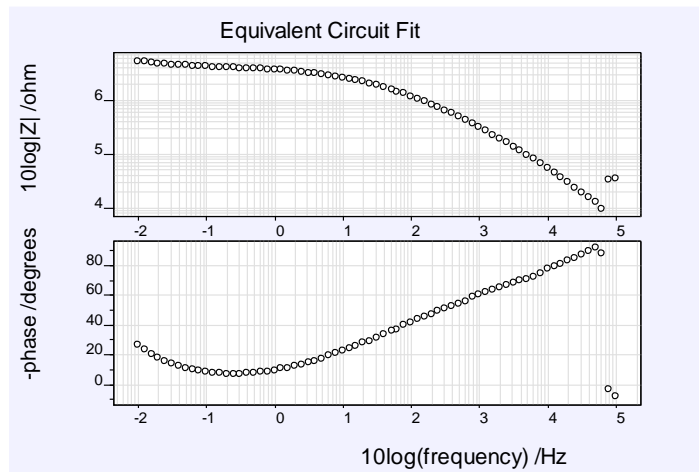


Figure 12. Bode plot of coated AA 2024 in pH 7.9 at 30 °C

Nyquist plots also show highly similar responses, a capacitive loop followed by a tail for pH 6 and 7.9 of the experiments. This tail that originates from diffusion, disappears when solution pH is at its highest level, 9.5.

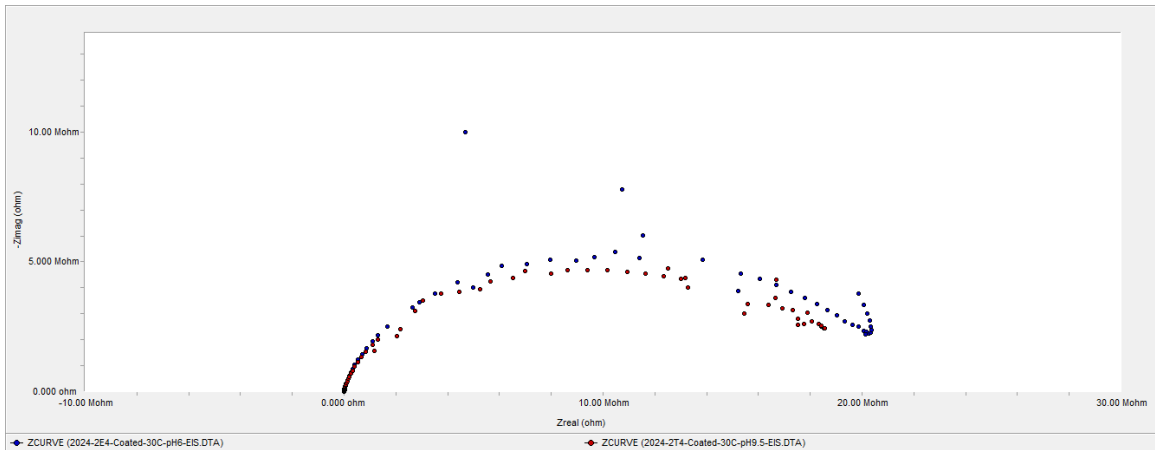


Figure 13. Nyquist plots of coated AA 2024 in pH 6 and pH 9.5 at 30 °C

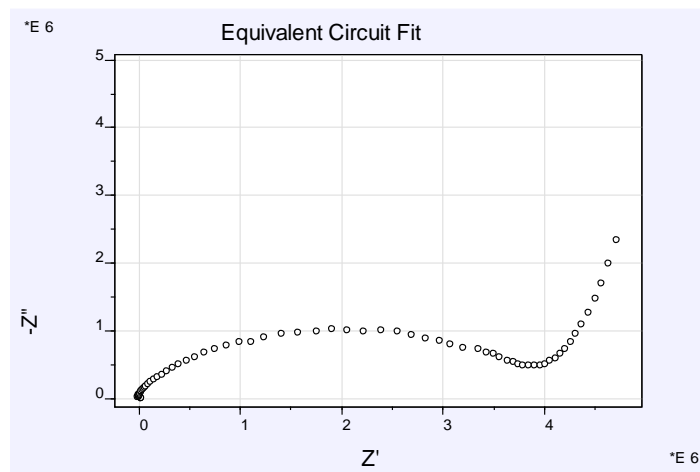


Figure 14. Nyquist plot of coated AA 2024 in pH 7.9 at 30 °C

Figure 15 to 18 show Bode plots and Nyquist plots of bare AA 2024-T3 tested in temperature of 30 °C for the varying pH. As the test for pH 7.9 has done in a different potentiostat (Evium), the graphs of the data are presented separately. In this part, plots for both Bode and Nyquist diagrams seem a bit different than each other, although this difference is more highlighted in Nyquist plots. In Bode plot, graphs are fairly similar in shape in range of high frequency to near one hertz. From one hertz to the lower end of frequency, for pH of 7.9 and 9.5, plots become a straight line, characteristic of resistive behavior, for a short interval and again impedance start to increase. This capacitive behavior can be related to the presence of the double layer capacitance in the circuit. When pH of the solution is 6, at lower frequency than one hertz, there is an inductive behavior which correspond to the diffusion on the metal surface.

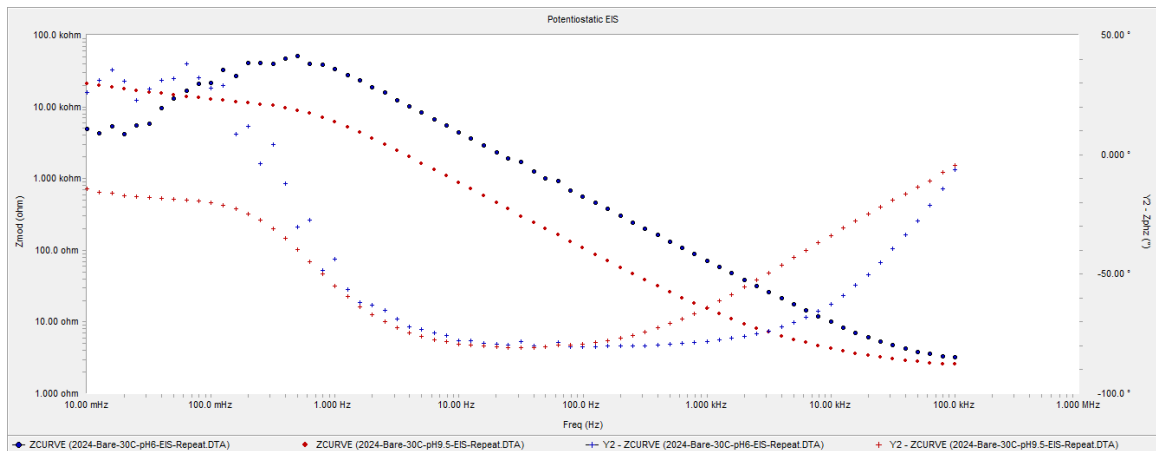


Figure 15. Bode plots of bare AA 2024 in pH 6 and pH 9.5 at 30 °C

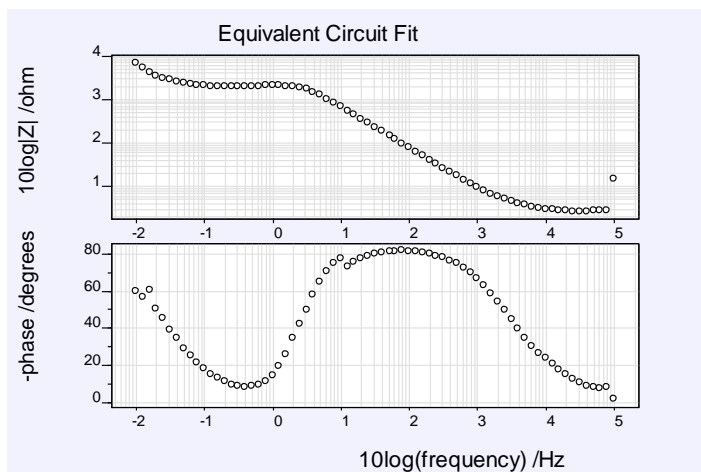


Figure 16. Bode plot of bare AA 2024 in pH 7.9 at 30 °C

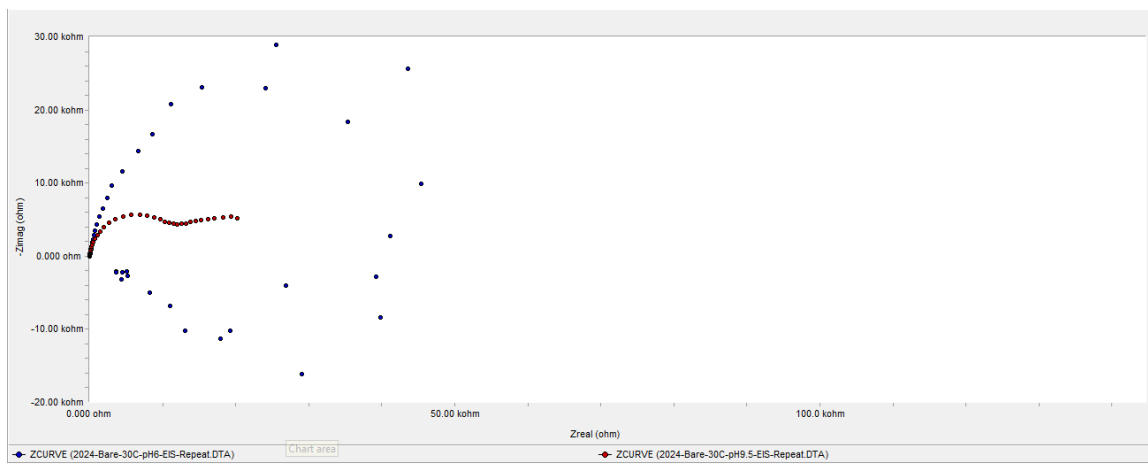


Figure 17. Nyquist plots of bare AA 2024 in pH 6 and pH 9.5 at 30 °C

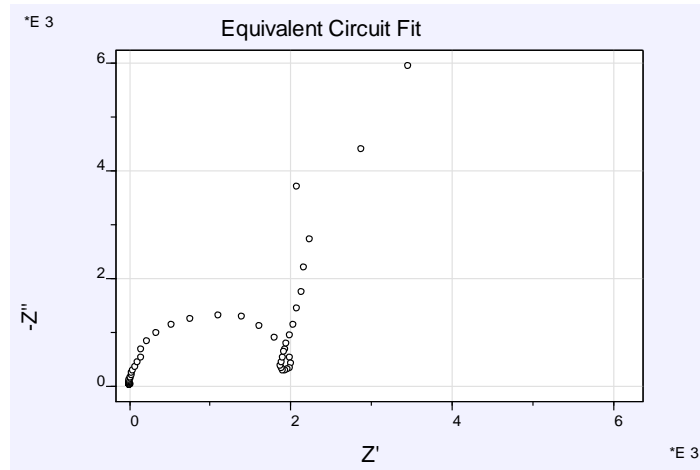


Figure 18. Nyquist plot of bare AA 2024 in pH 7.9 at 30 °C

Figure 19 to 22 show Bode plots and Nyquist plots of coated AA 2024-T3 tested in temperature of 40 °C for three different pH. As it can be seen from the Bode plots, the shapes of the graphs for all three cases are fairly similar. From the highest frequency a capacitive behavior is observed which last to about one hundred hertz. This capacitive behavior is followed by a resistive horizontal line, indication of charge transfer resistance, until one hundred mHz. The resistive behavior turns to a capacitive one again to the lower end of frequency. The frequency does not go high sufficiently to show the resistance of the solution. The Nyquist diagrams also present identical shapes for all three cases. They appear as a capacitive loop followed by a tail for each pH, indication of diffusion on the metal substrate. The biggest loop corresponds to the solution with highest pH, while the natural pH of seawater present the lowest protection.

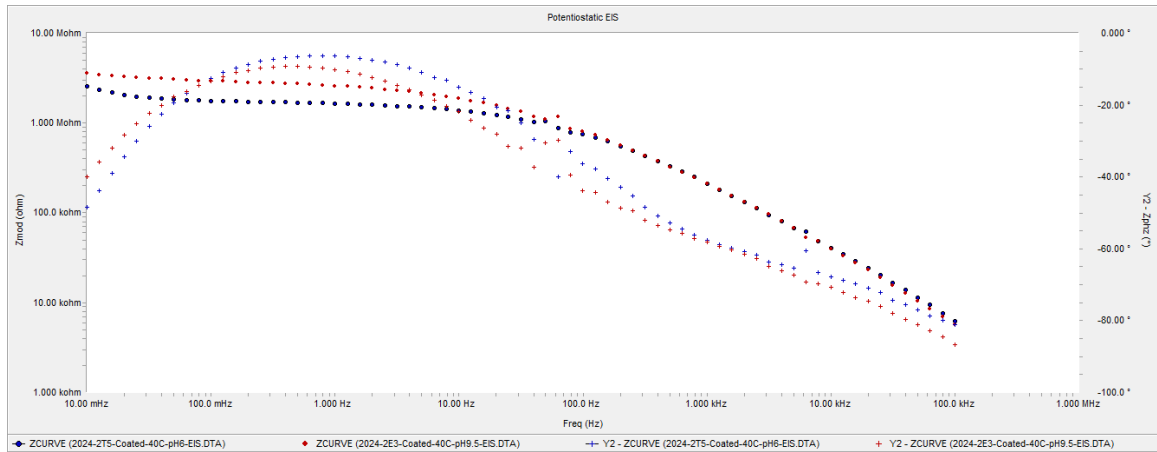


Figure 19. Bode plots of coated AA 2024 in pH 6 and pH 9.5 at 40 °C

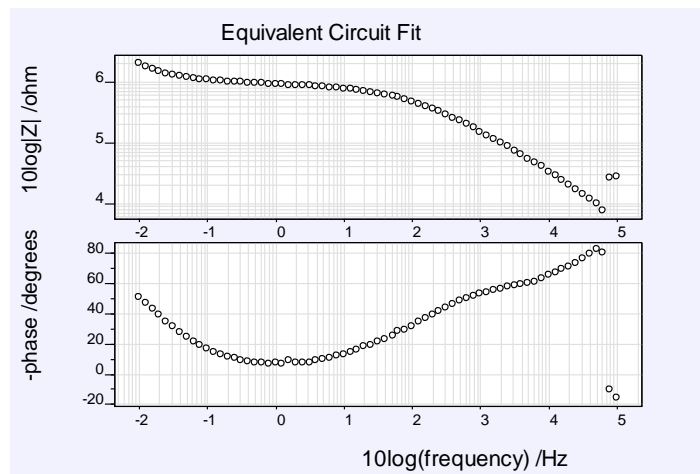


Figure 20. Bode plot of coated AA 2024 in pH 7.9 at 40 °C

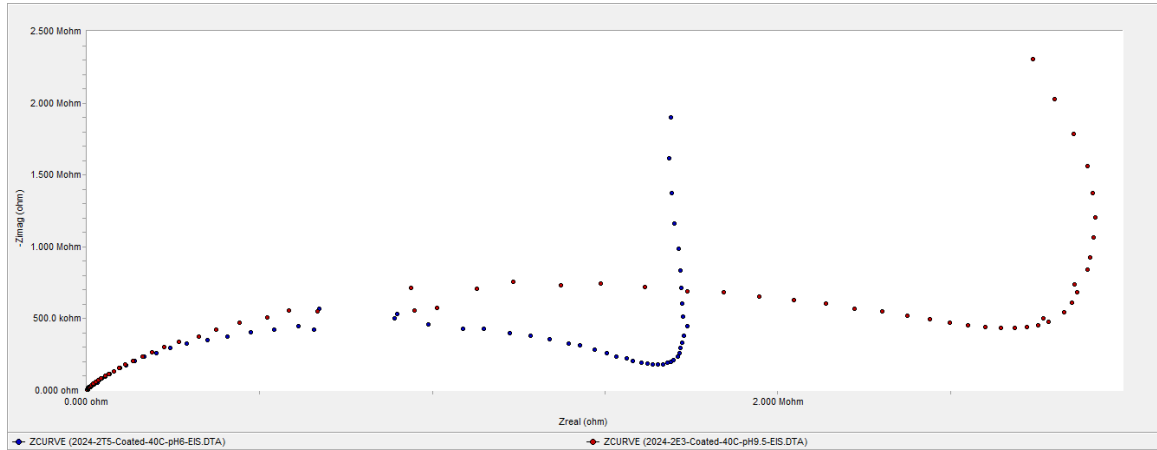


Figure 21. Nyquist plots of coated AA 2024 in pH 6 and pH 9.5 at 40 °C

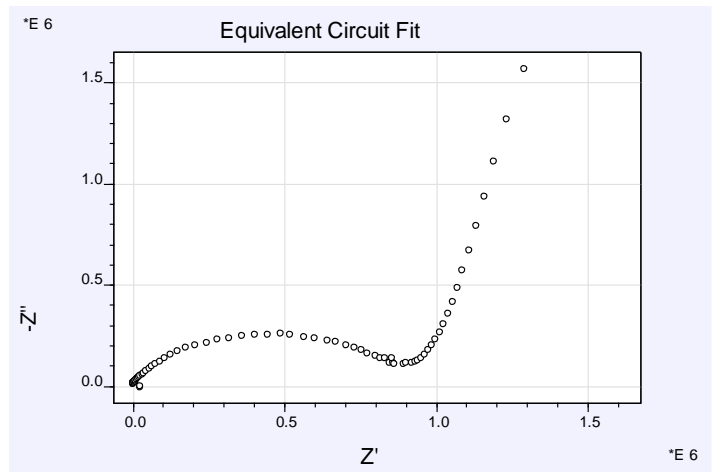


Figure 22. Nyquist plot of coated AA 2024 in pH 7.9 at 40 °C

Figure 23 to 26 show Bode plots and Nyquist plots of bare AA 2024-T3 tested in temperature of 40 °C for three different pH. As it can be seen the plots show different behavior for each pH. In acidic seawater one time constant is seen followed by an inductive

behavior in low frequency. In natural pH of seawater, a capacitive semi-circle is formed followed by another depressed capacitive loop. The first semi-circle indicates the breakdown of the oxide layer and the second one corresponds to the smaller time constant in the equivalent circuit. In the basic seawater also two semi-circles are observed. At the highest temperature of the experiment, the acidic seawater shows the highest protection.

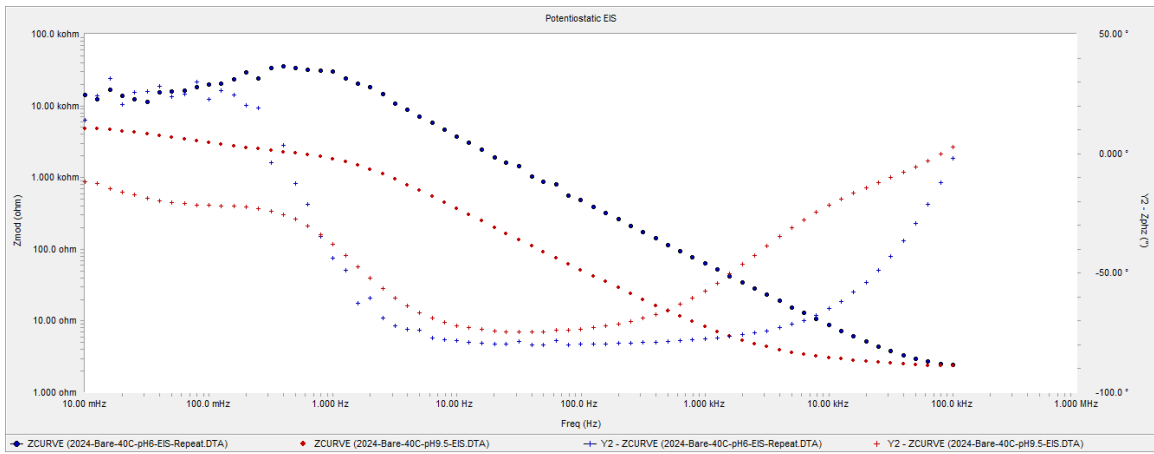


Figure 23. Bode plots of bare AA 2024 in pH 6 and pH 9.5 at 40 °C

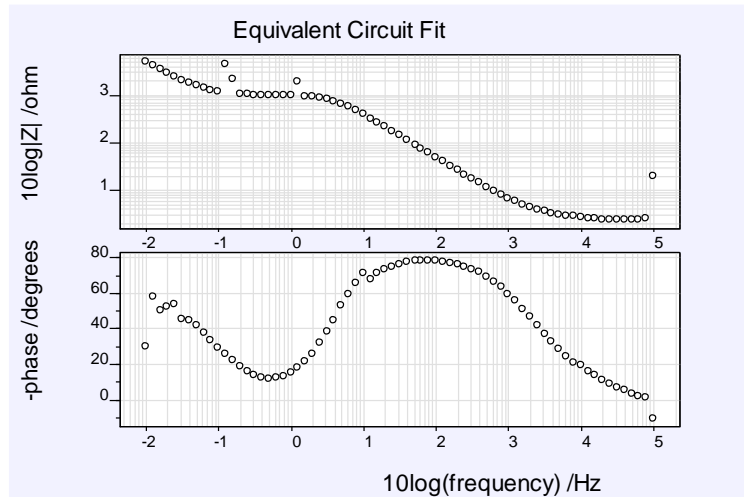


Figure 24. Bode plot of bare AA 2024 in pH 7.9 at 40 °C



Figure 25. Nyquist plots of bare AA 2024 in pH 6 and pH 9.5 at 40 °C

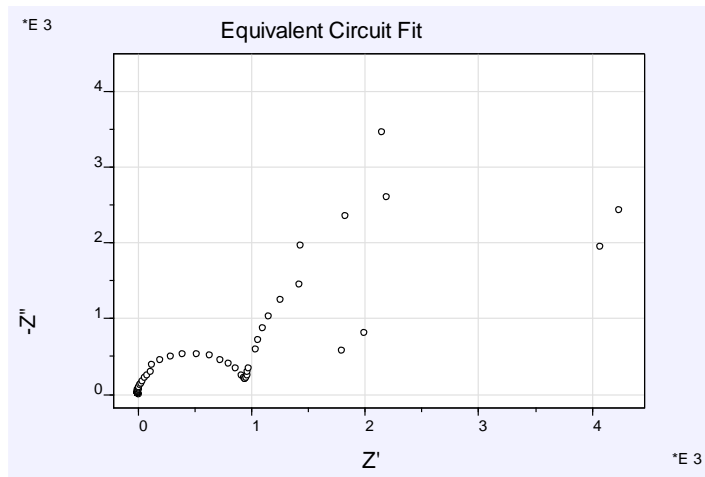


Figure 26. Nyquist plot of bare AA 2024 in pH 7.9 at 40 °C

4.2. Polarization Resistance Tests

4.2.1. Tafel Tests on Bare and Coated Aluminum Alloy 2024-T3

Figure 27 shows the effect of increasing temperature on corrosion rates for bare AA 2024. The graph contains the three temperatures and pH used in the experiments. The results for the bare alloy show that decreasing pH from 9.5 to 6 at 20 °C slightly increases the corrosion rate. This also holds for 30 °C with slight difference. The protective nature and composition of the corrosion product depend greatly on the pH of the solution. Figure 32 illustrates that the corrosion rate for all pH remains almost stable with increasing the temperature from 20 to 30 °C. Interestingly, as temperature is elevated to 40 °C, corrosion rates for pH of 7.9 and 9.5 change significantly and increase one order of magnitude. This dramatic increase in corrosion rate can be explained by acceleration of diffusion of species involved in electrochemical reactions due to temperature increase. Another reason is that temperature by evaporating one or more species out of the solution could affect the concentration of corrosion species, which in turn could affect the corrosion reaction. Further, previous studies have proved that temperature generally accelerates most of the chemical, electrochemical and transporting processes occurring during the corrosion process. With increasing temperature, also, both cathodic reactions and anodic currents were measured to increase [41]. This change for pH of 6 appears decreasing and not as significant as higher pH. As it can be clearly seen, at 40 °C the highest corrosion rate belongs to natural pH of seawater and the lowest corrosion occurs in the lowest pH of experiment, pH of 6.

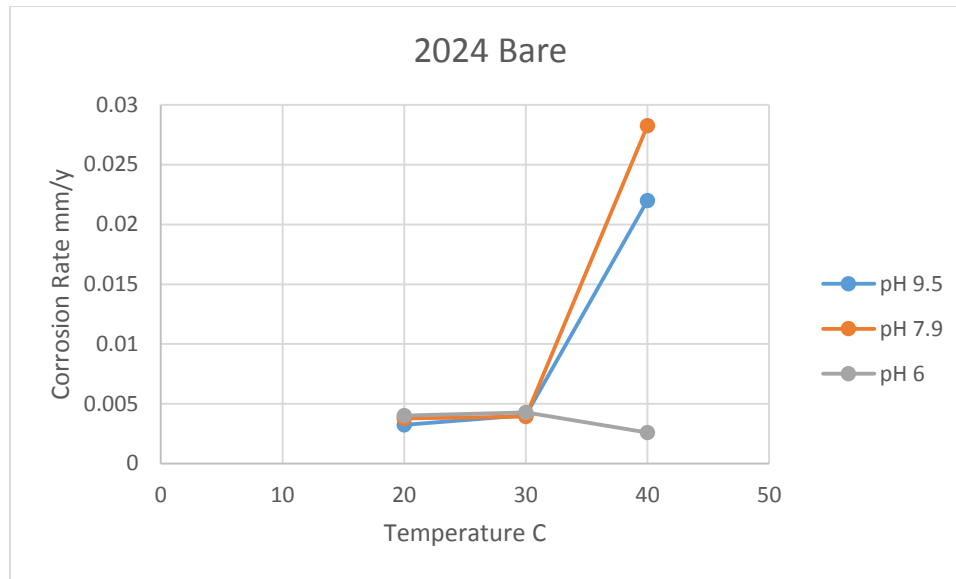


Figure 27. The corrosion rate of bare AA 2024-T3 at different temperatures and pH

Figure 28 shows the effect of increasing temperature on the corrosion rate of the coated AA 2024 specimens at different pH.

It is observed that there is a stable increase of corrosion rate for each pH with elevation of the temperature. When coated, the acidic solution shows the highest metal dissolution at room temperature, while natural pH of seawater provide the highest protection. This behavior becomes inverse as temperature increases, such that the natural pH of seawater significantly increases and stands on the top in the list for corrosion rate at 30 °C. Further increase of temperature from 30 to 40 °C, keeps the natural pH of seawater still on the top resulting in highest corrosion rate. It should be noted that at the highest level of temperature in the experiments, the highest pH shows the lowest corrosion rate for coated samples of

AA 2024. Needless to say, the coating system has provided excellent protection to the alloy when compared with the bare metals in the experiment.

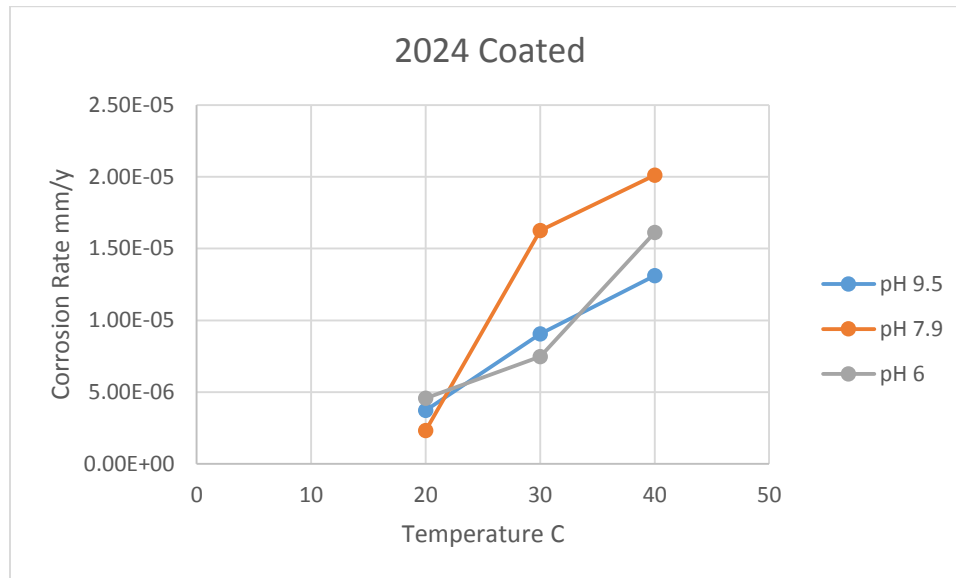


Figure 28. The corrosion rate of coated AA 2024-T3 at different temperatures and pH

4.2.2. Tafel Tests on Bare and Coated Aluminum Alloy 7075-T6

Figure 29 shows the effect of increasing temperature on corrosion rates for bare AA 7075. The graph contains the three temperatures and three pH used in the experiments. The results for the bare alloy show that decreasing pH from 9.5 to 6 at room temperature does not necessarily increase the corrosion rate. This is demonstrated by the fact that the natural pH of seawater has the lowest corrosion rate rather than pH 9.5 at 20 °C. This situation also holds for pH 7.9 at 30 °C, but unlike 20 °C, the highest corrosion rate corresponds to an alkaline solution rather than an acidic one. When the temperature is elevated to 40 °C, similar to AA 2024, corrosion rates change significantly. Interestingly, the pattern of changes

exactly follow those of for AA 2024; corrosion rate for acidic pH decreases and the ones for natural pH of seawater and highly basic medium increases remarkably. Likewise, at 40 °C, the highest corrosion rate happens in natural pH of seawater, and the lowest corrosion occurs in the acidic seawater.

As it said before, this dramatic increase in corrosion rate can be explained by either by acceleration of diffusion of species involved in electrochemical reactions due to temperature increase or by evaporation of species out of the solution and subsequent change of concentration of corrosion species.

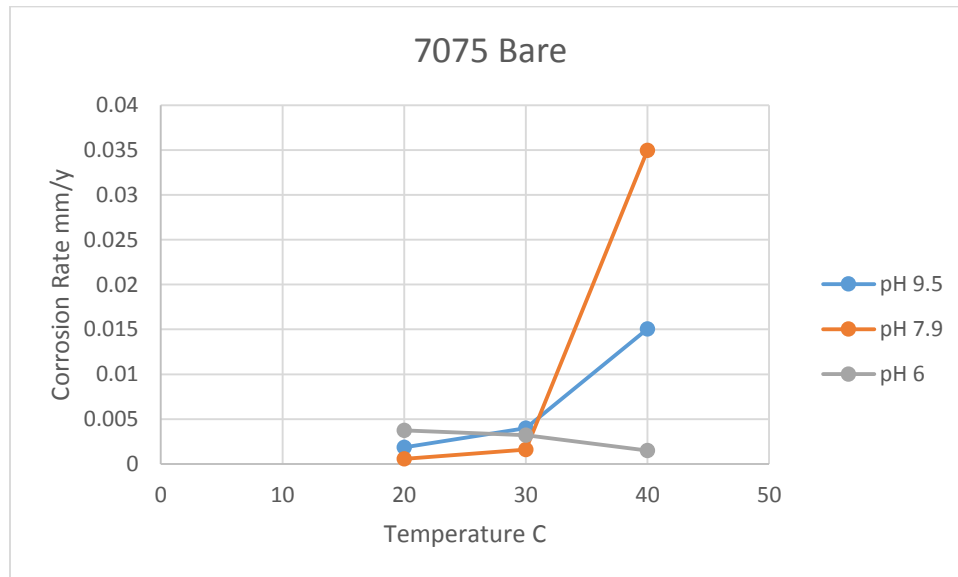


Figure 29. The corrosion rate of bare AA 7075-T6 at different temperatures and pH

Figure 30 shows the effect of increasing temperature on the corrosion rate of the epoxy coated AA 7075 specimens at different pH. The graph indicates stable behavior of anodic dissolution curves with increasing the temperature from 20 to 40 for all three pH involved in the experiment. The acidic seawater holds the lowest corrosion rate throughout the experiment for coated AA 7075. At room temperature pH 9.5 attributes to the most destructive corrosion, while natural pH of seawater stands on the second place. As temperature elevates pH 7.9 shows the highest corrosion rate for both 30 °C and 40 °C. Interestingly, this behavior is pretty similar to that of coated AA 2024. A simple comparison makes that obvious that the coating system protects the metal substrate effectively for all combination of pH and temperatures.

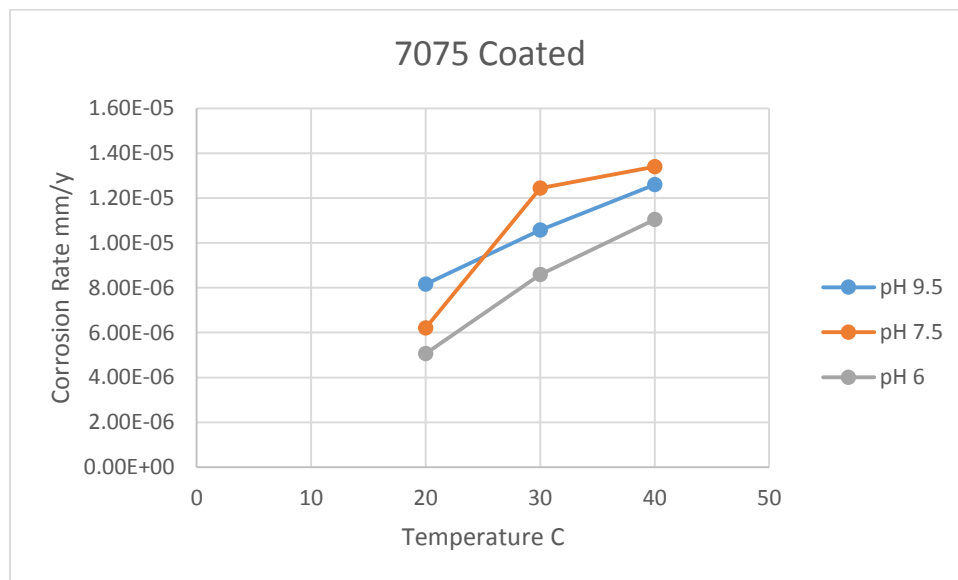


Figure 30. The corrosion rate of coated AA 7075-T6 at different temperatures and pH

Chapter 5

Conclusion

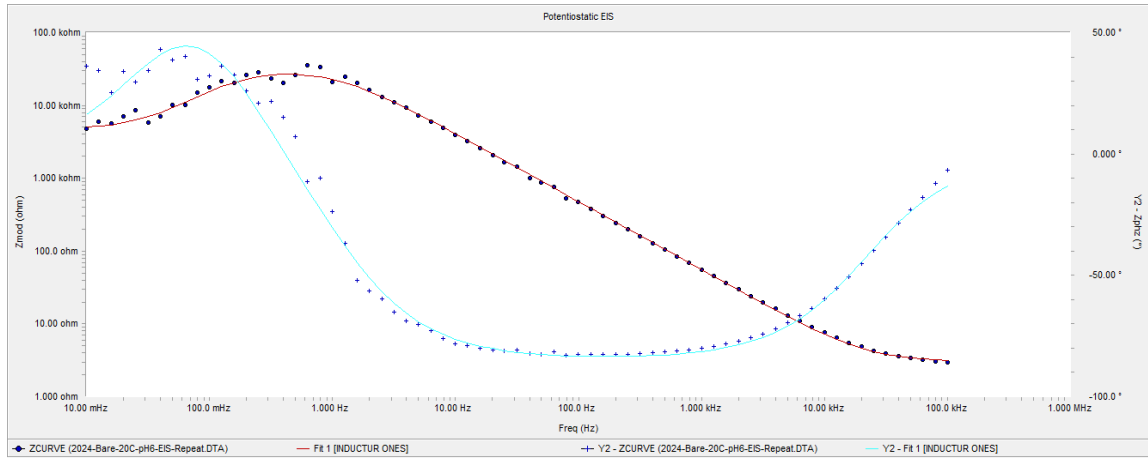
In this research efficiency of a two-layer coating system, zinc-phosphate and epoxy, has been tested by electrochemical impedance spectroscopy and polarization resistance techniques. EIS test results show that the selected coating system acts closely to a pure capacitor in first hour of immersion. This, simply, means that the coating perfectly protects the alloy substrate against seawater in all temperatures and pH involved in the study. To get a better resolution on protectiveness of the coating system in environment with varying conditions, time parameter should be considered as one of the variables in experiments for later research.

Also, the results of tafel test indicate that as temperature increases, corrosion rate also increase steadily. Further, at elevated temperatures the natural pH of the seawater, pH 7.9, has the most detrimental effect on the coating system. A comparison between polarization resistance tests performed on bare and coated alloys indicate that corrosion is decreased to several order of magnitude. In this research, lack of equipment for accurately coating the samples and consequent inconsistency of coating layers and thickness may have attributed to some errors in the results. Further inevitable noises and vibrations may have resulted in errors during electrochemical measurements. Accordingly, the results should not be considered as exact values, but for comparison.

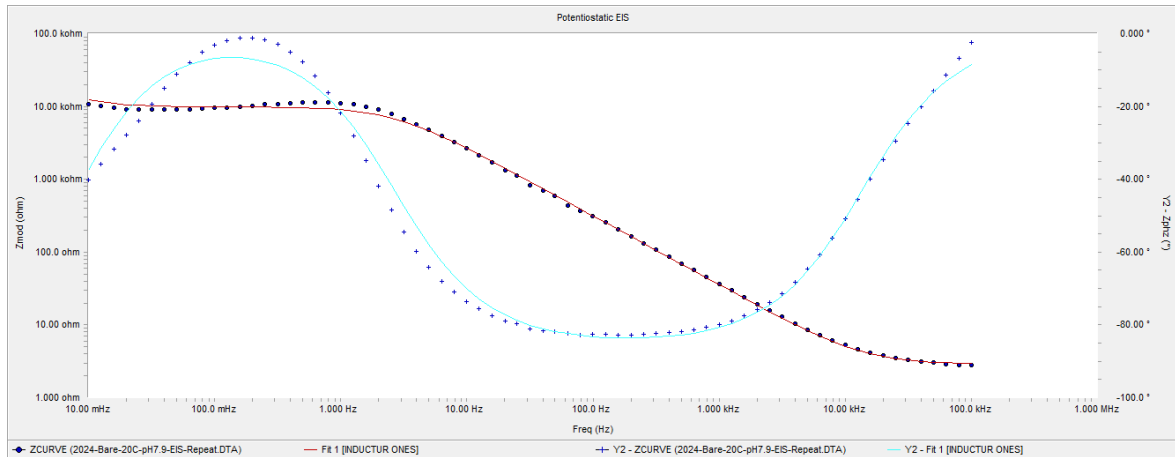
Future Work

In this research, the effect of immersion time has not been studied, and the variables of the experiments include pH and temperature. To get a better resolution on the coating performance, it is highly beneficial to consider varying immersion times as well as other parameters. One common practice in this regard is immersing the coated samples into the different corroding solutions and performing EIS tests periodically. This periodic measurements benefits the research through providing information about coating degradation by time, which in turn could be used for taking further safety measurements such as predictive maintenance.

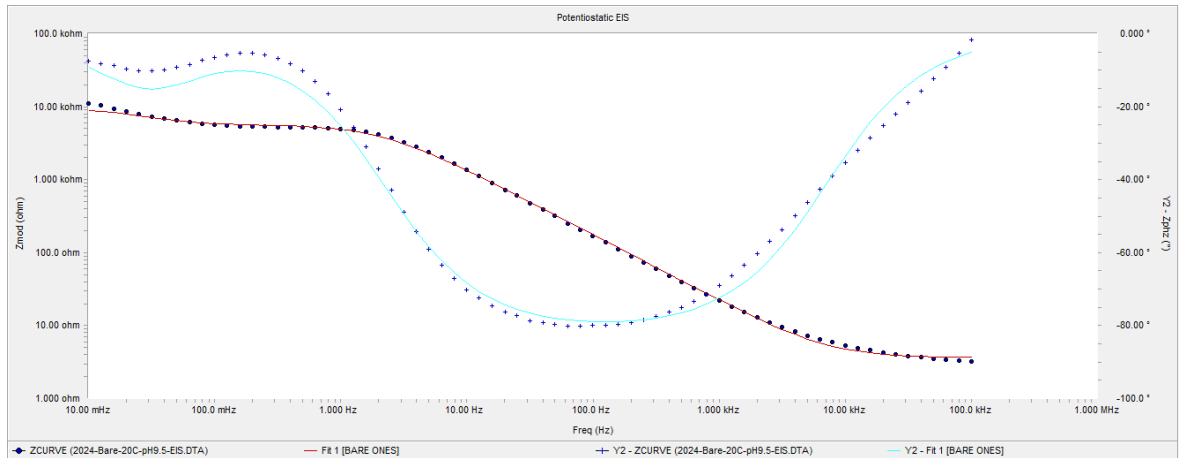
APPENDIX: Fit of EIS data to equivalent circuit



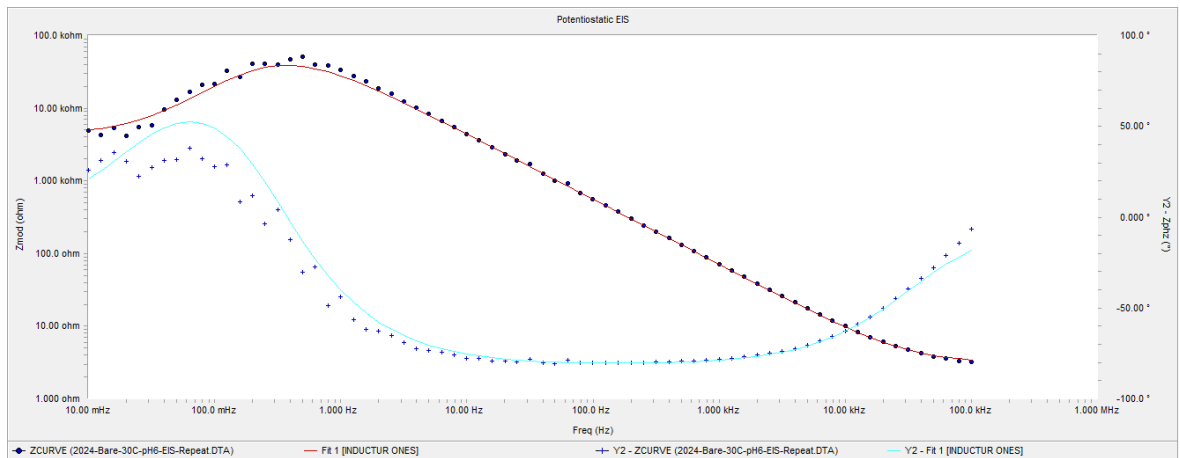
A 1. The bode plot diagram of bare AA 2024-T3 sample at 20 °C and pH 6



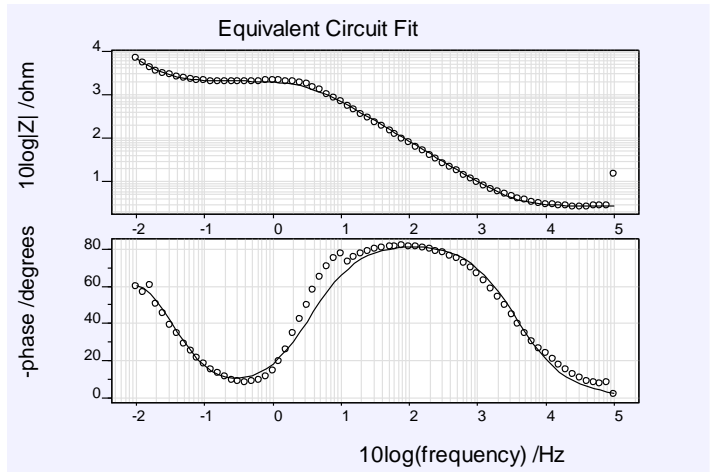
A 2. The bode plot diagram of a bare AA 2024-T3 sample at 20 °C and pH 7.9



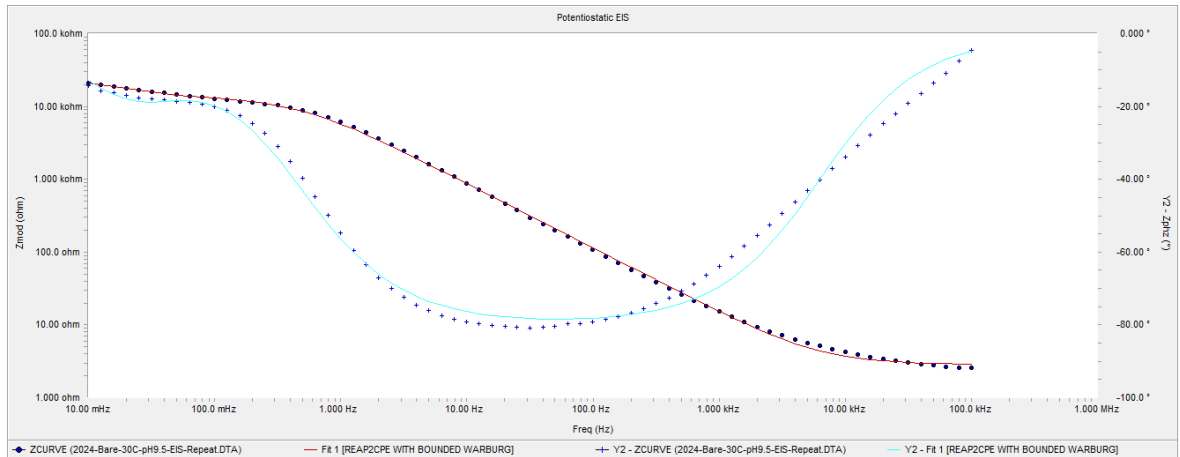
A 3. The bode plot diagram of a bare AA 2024-T3 sample at 20 °C and pH 9.5



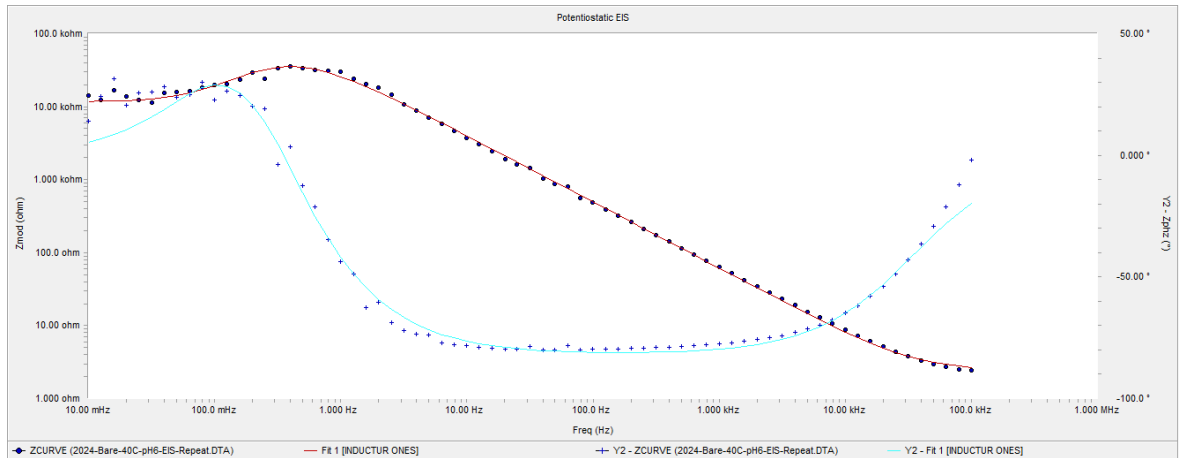
A 4. The bode plot diagram of a bare AA 2024-T3 sample at 30 °C and pH 6



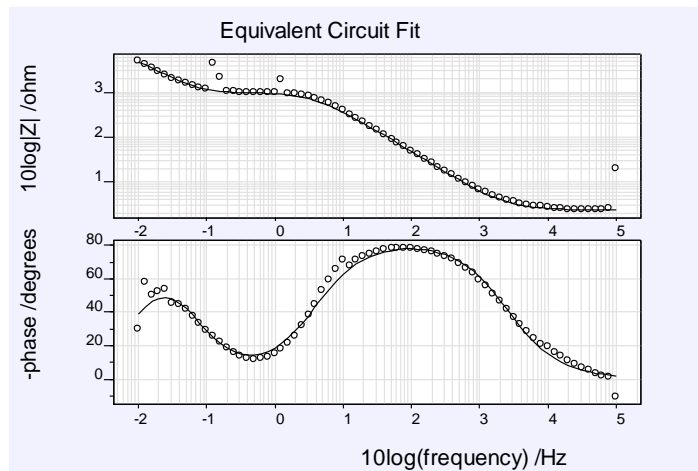
A 5. The bode plot diagram of a bare AA 2024-T3 sample at 30 °C and pH 7.9



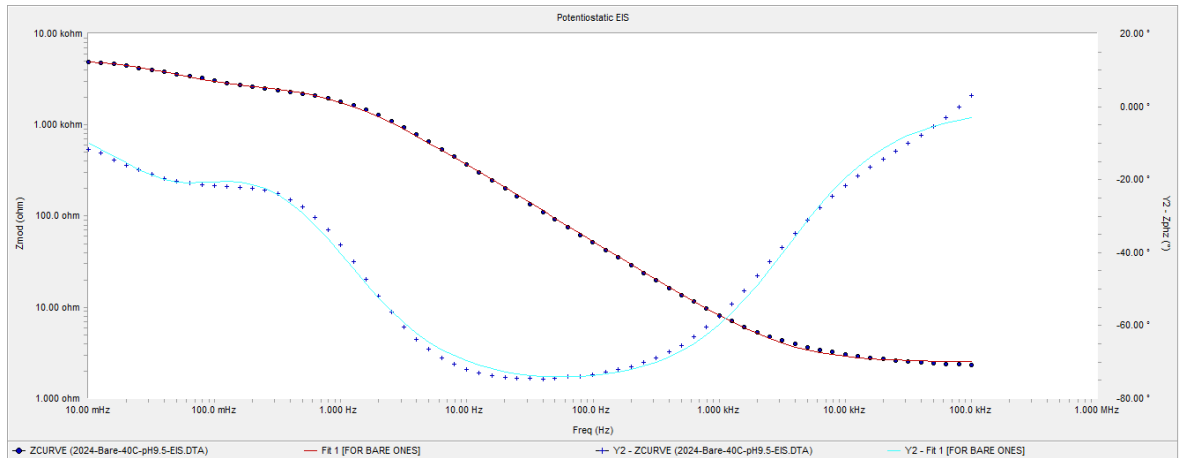
A 6. The bode plot diagram of a bare AA 2024-T3 sample at 30 °C and pH 9.5



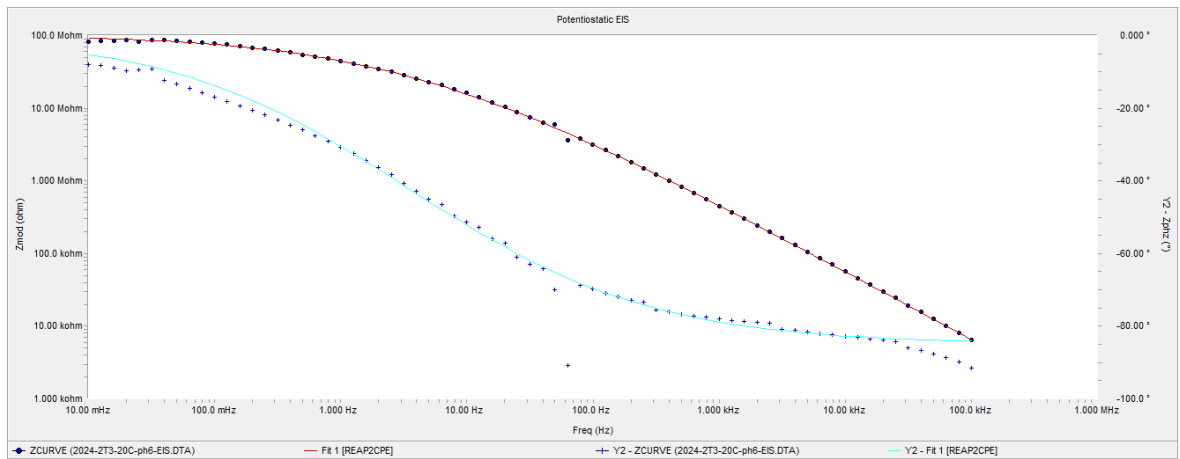
A 7. The bode plot diagram of a bare AA 2024-T3 sample at 40 °C and pH 6



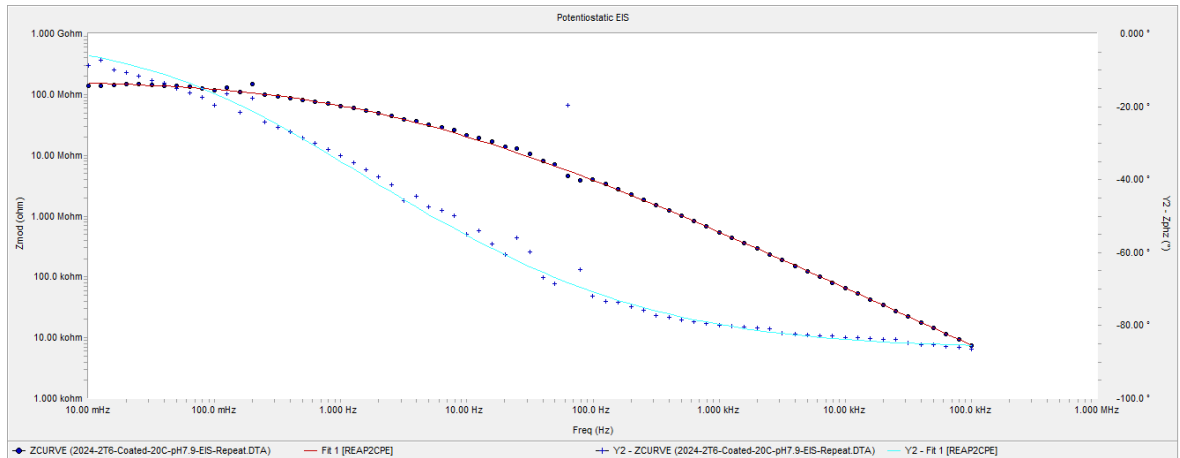
A 8. The bode plot diagram of a bare AA 2024-T3 sample at 40 °C and pH 7.9



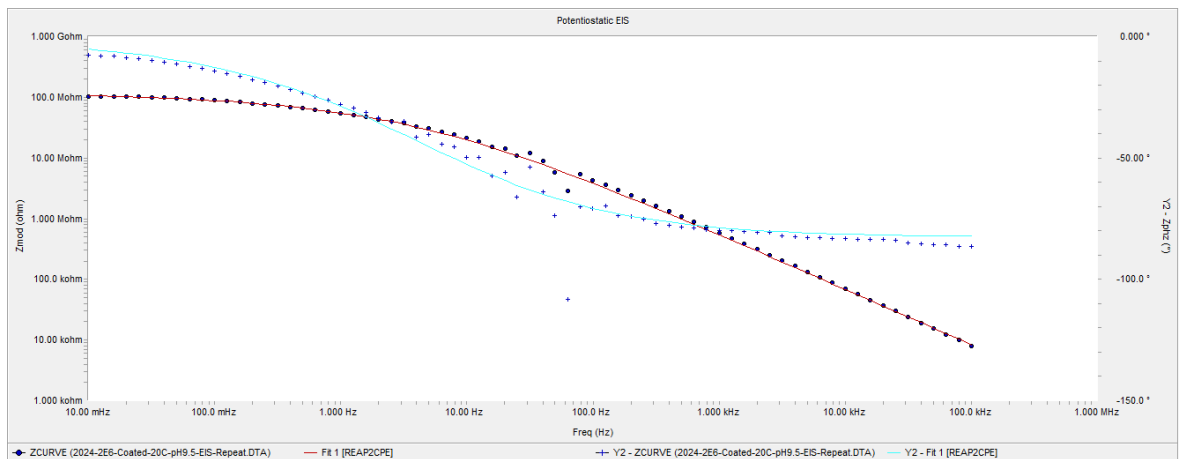
A 9. The bode plot diagram of a bare AA 2024-T3 sample at 40 °C and pH 9.5



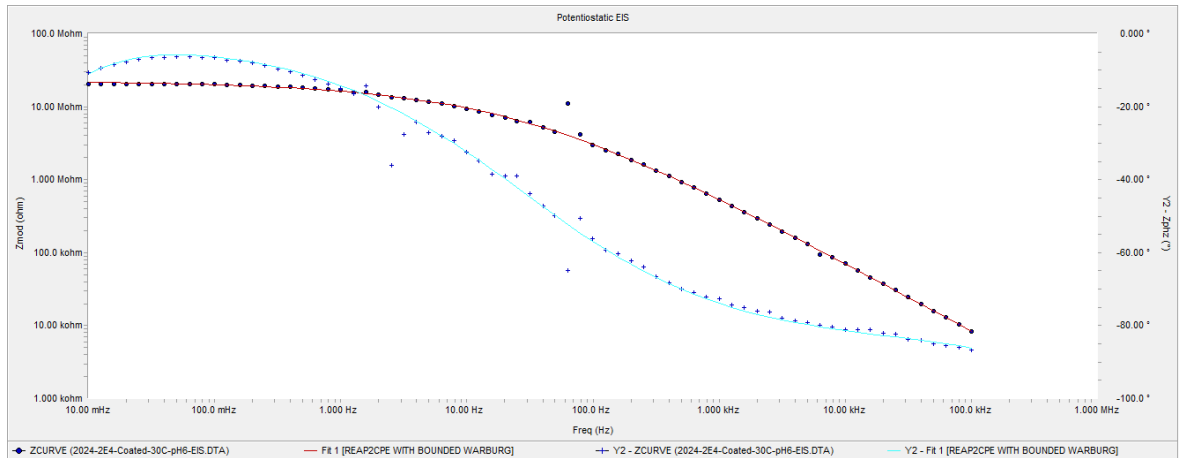
A 10. The bode plot diagram of a coated AA 2024-T3 sample at 20 °C and pH 6



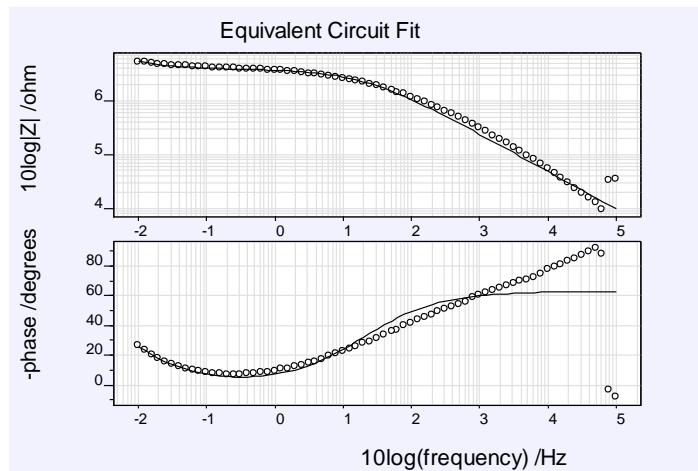
A 11. The bode plot diagram of a coated AA 2024-T3 sample at 20 °C and pH 7.9



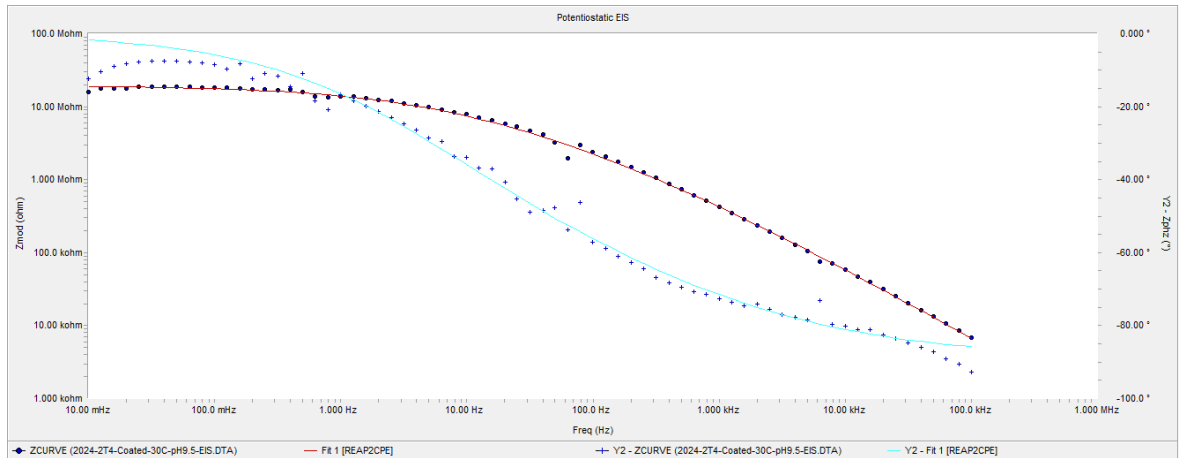
A 12. The bode plot diagram of a coated AA 2024-T3 sample at 20 °C and pH 9.5



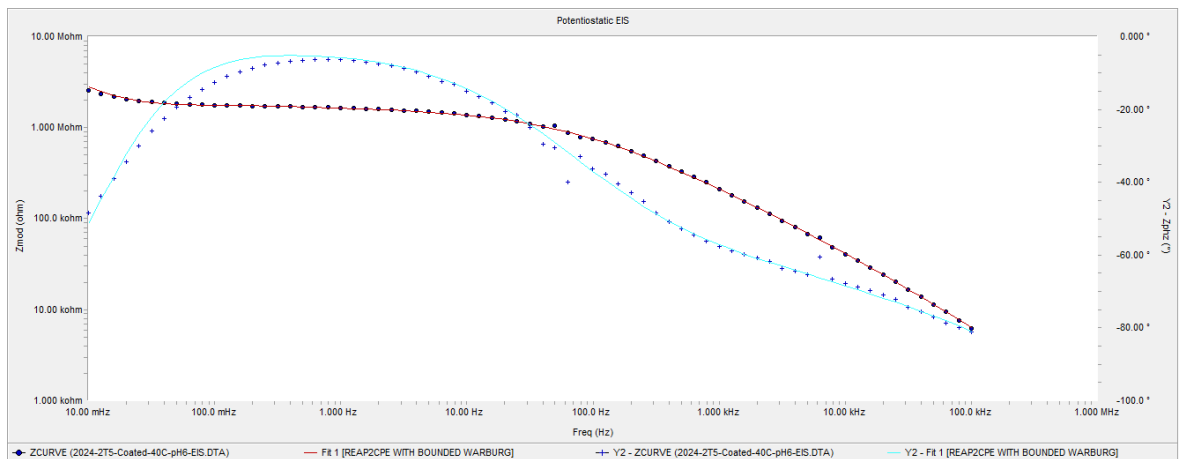
A 13. The bode plot diagram of a coated AA 2024-T3 sample at 30 °C and pH 6



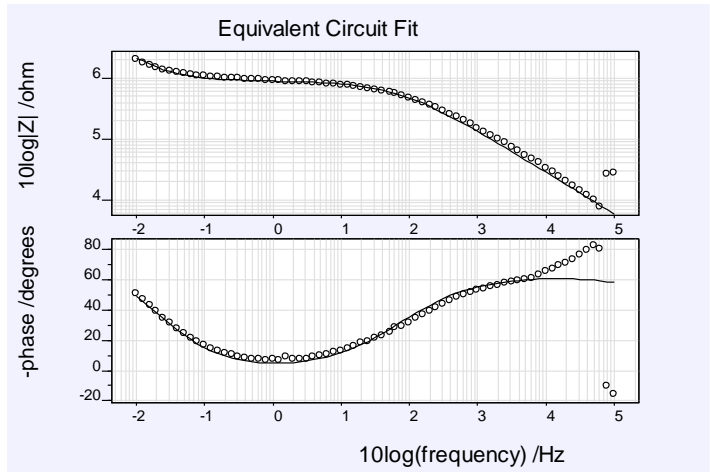
A 14. The bode plot diagram of a coated AA 2024-T3 sample at 30 °C and pH 7.9



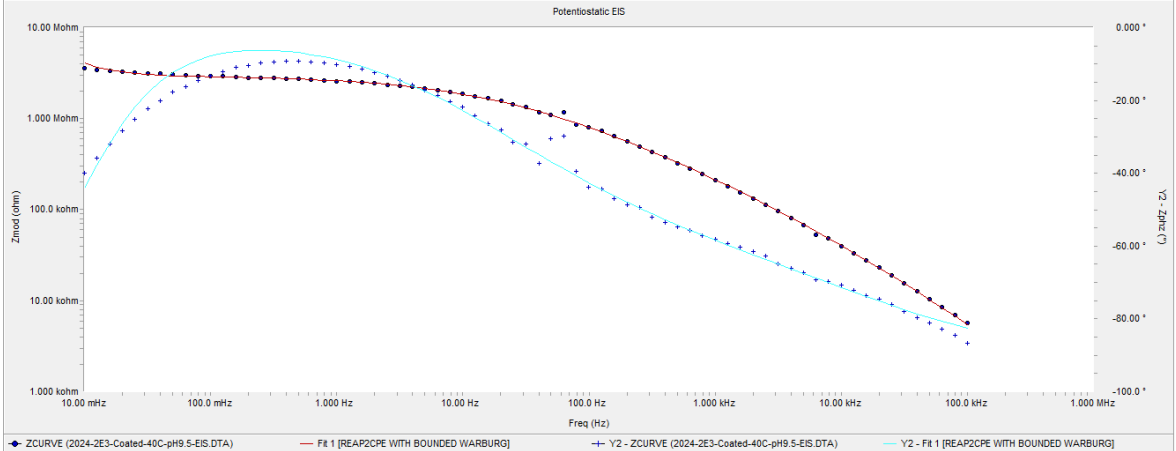
A 15. The bode plot diagram of a coated AA 2024-T3 sample at 30 °C and pH 9.5



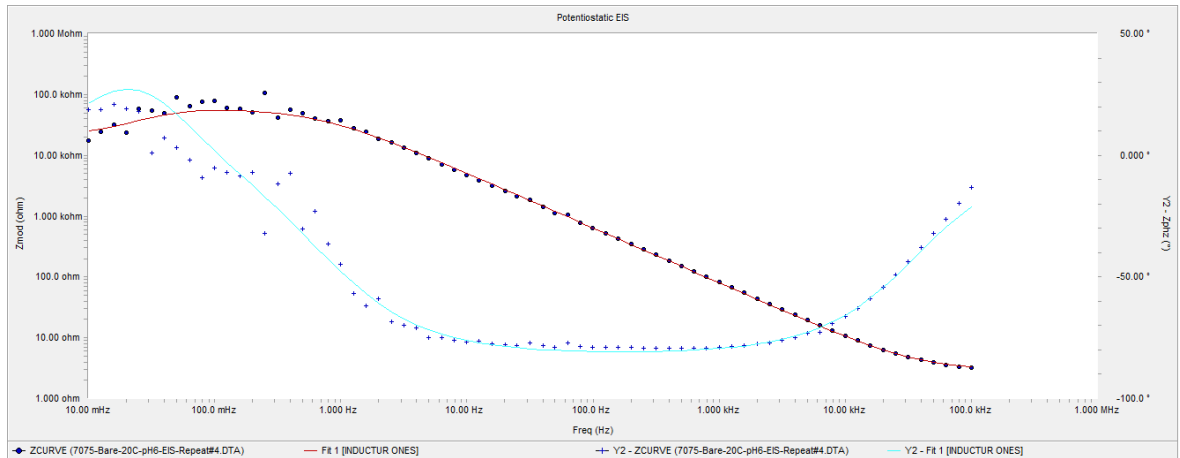
A 16. The bode plot diagram of a coated AA 2024-T3 sample at 40 °C and pH 6



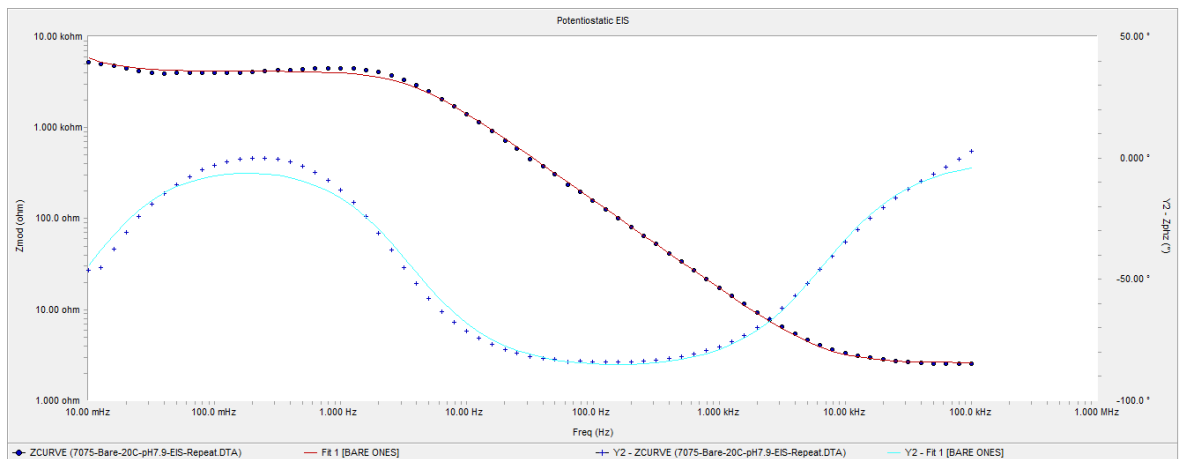
A 17. The bode plot diagram of a coated AA 2024-T3 sample at 40 °C and pH 7.9



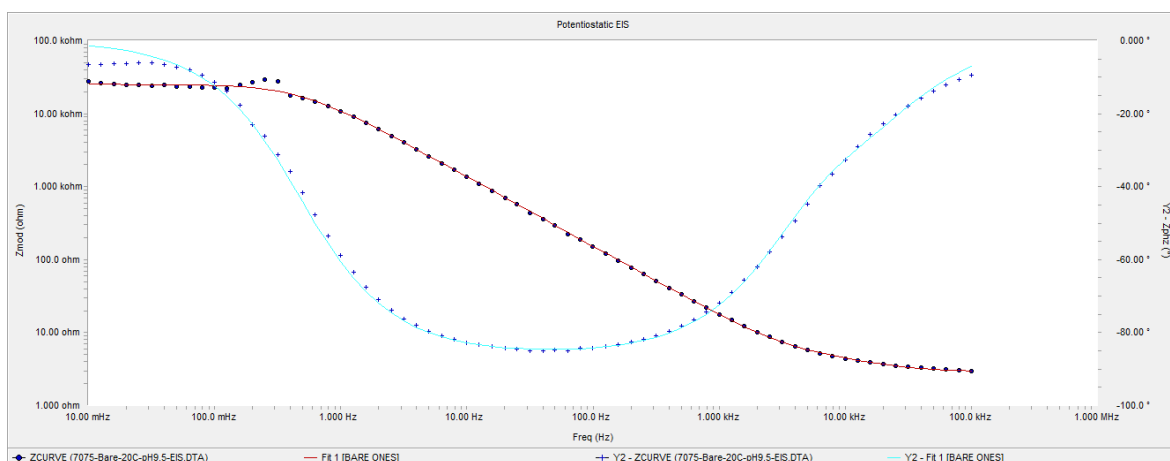
A 18. The bode plot diagram of a coated AA 2024-T3 sample at 40 °C and pH 9.5



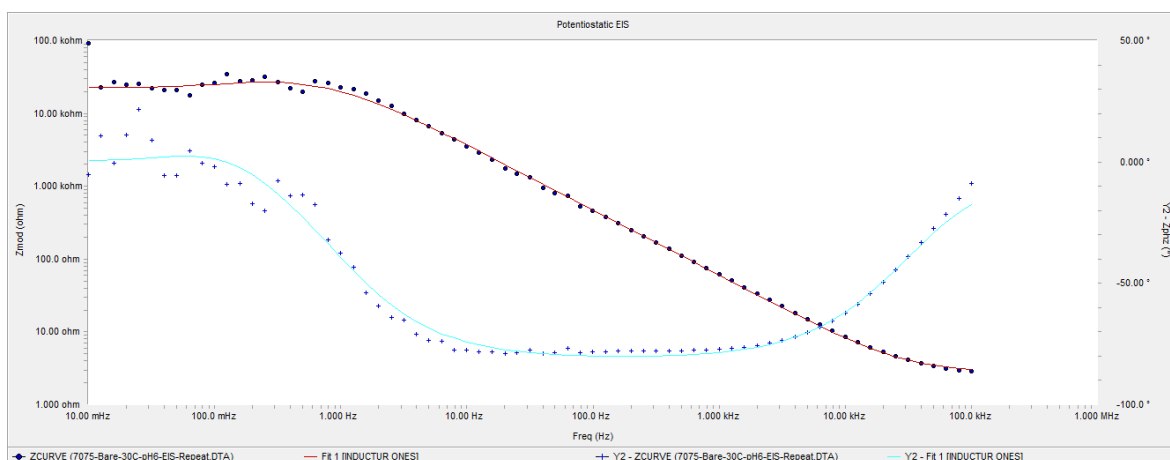
A 19. The bode plot diagram of a bare AA 7075-T6 sample at 20 °C and pH 6



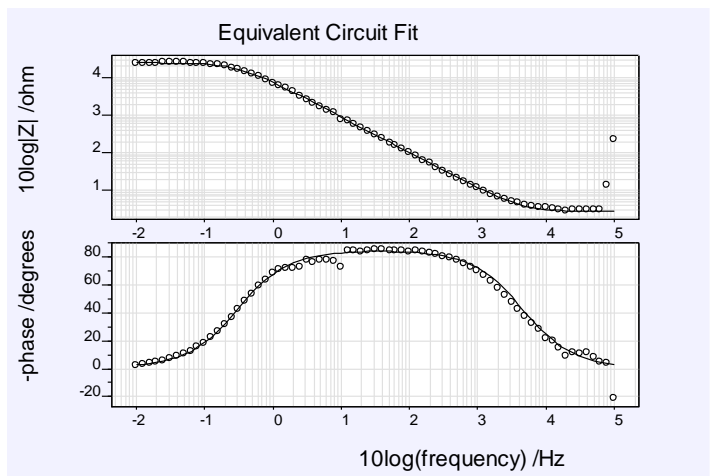
A 20. The bode plot diagram of a bare AA 7075-T6 sample at 20 °C and pH 7.9



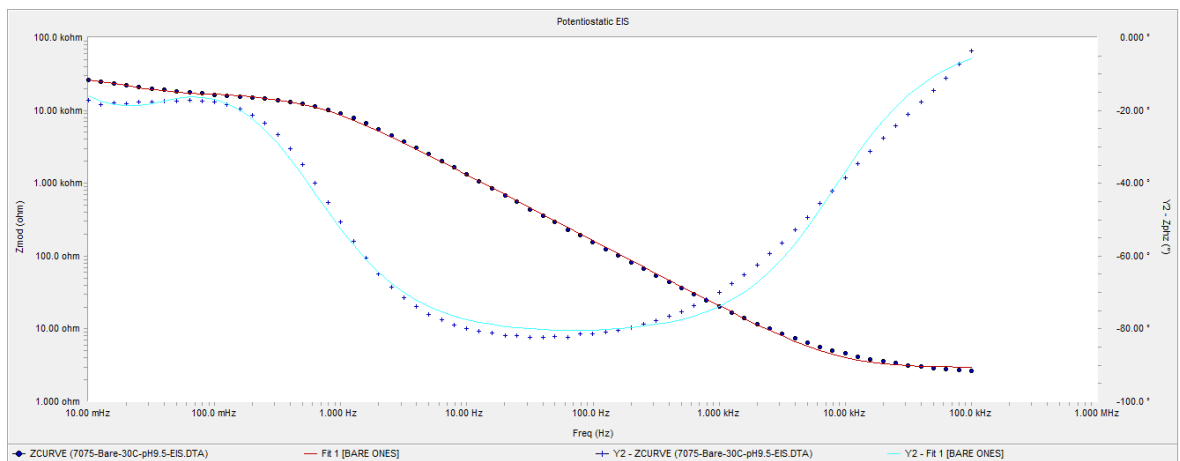
A 21. The bode plot diagram of a bare AA 7075-T6 sample at 20 °C and pH 9.5



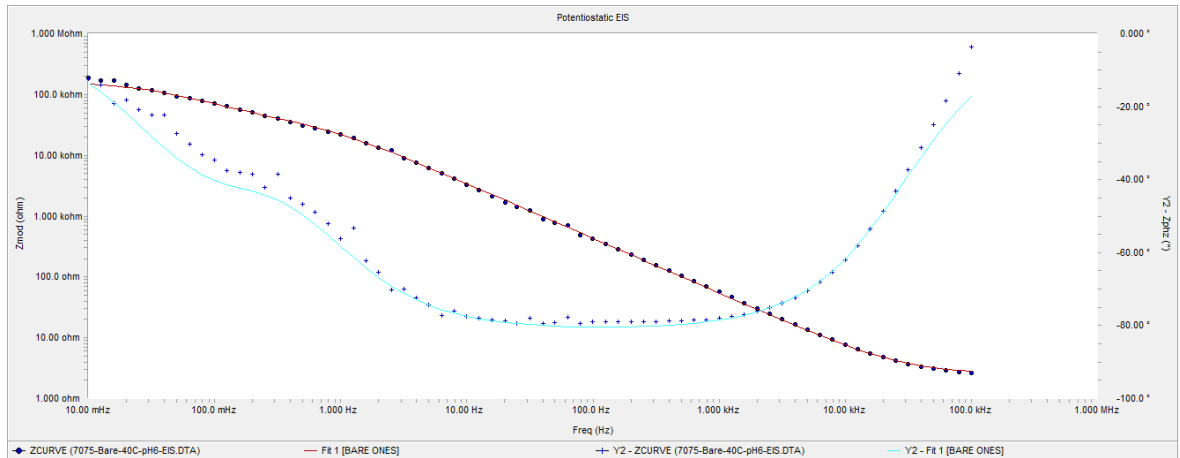
A 22. The bode plot diagram of a bare AA 7075-T6 sample at 30 °C and pH 6



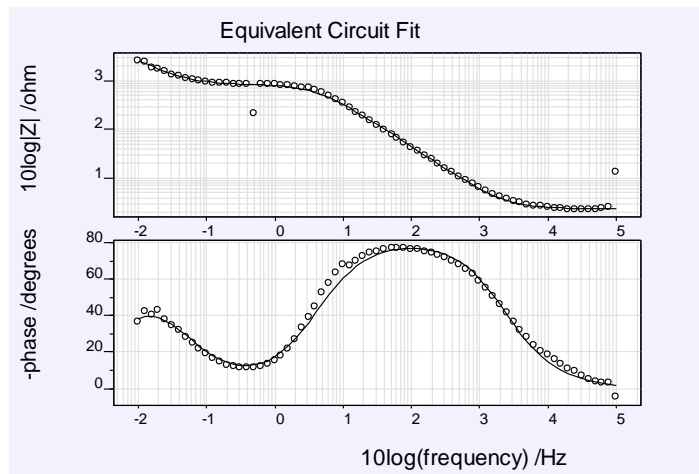
A 23. The bode plot diagram of a bare AA 7075-T6 sample at 30 °C and pH 7.9



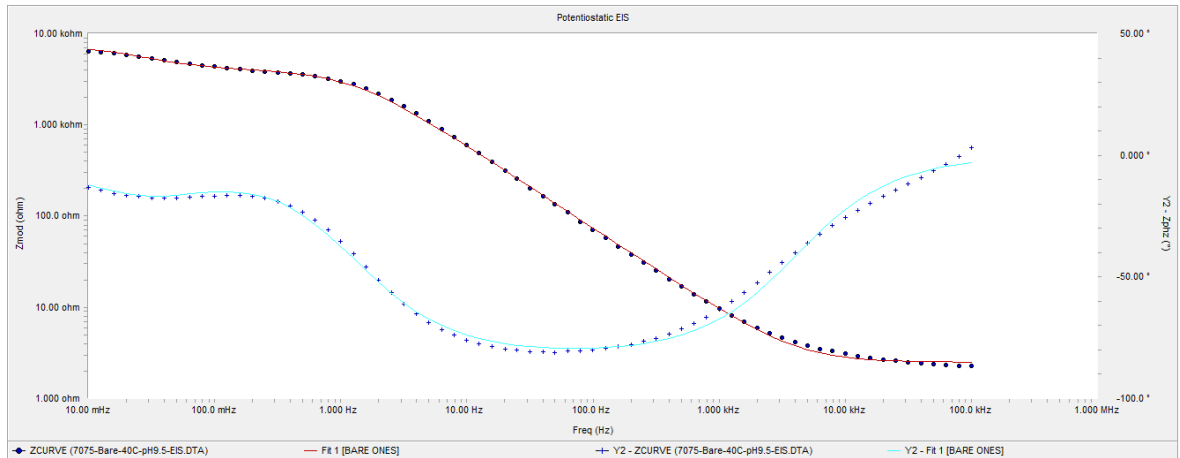
A 24. The bode plot diagram of a bare AA 7075-T6 sample at 30 °C and pH 9.5



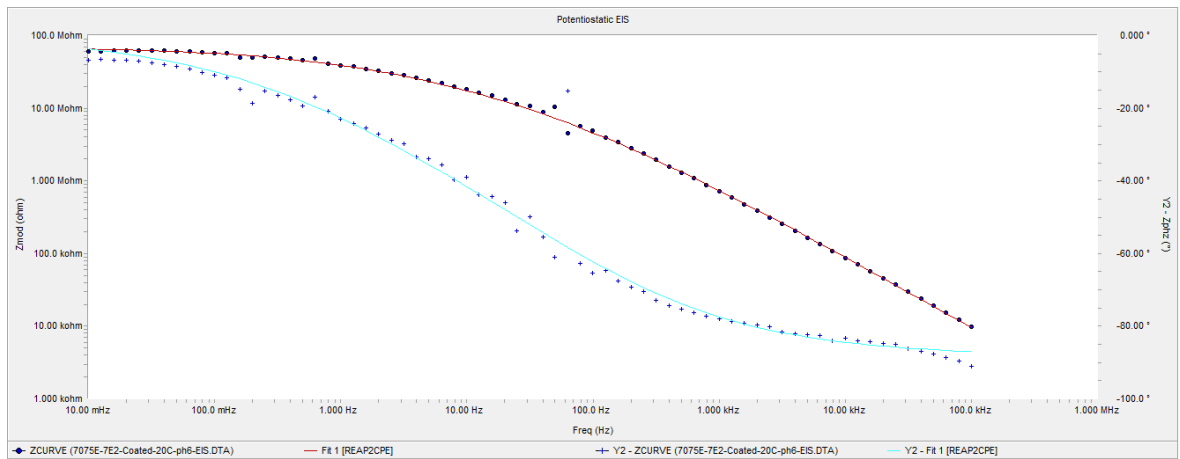
A 25. The bode plot diagram of a bare AA 7075-T6 sample at 40 °C and pH 6



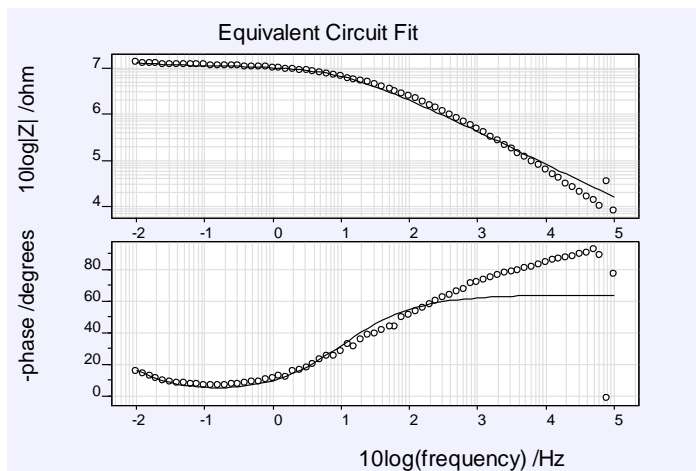
A 26. The bode plot diagram of a bare AA 7075-T6 sample at 40 °C and pH 7.9



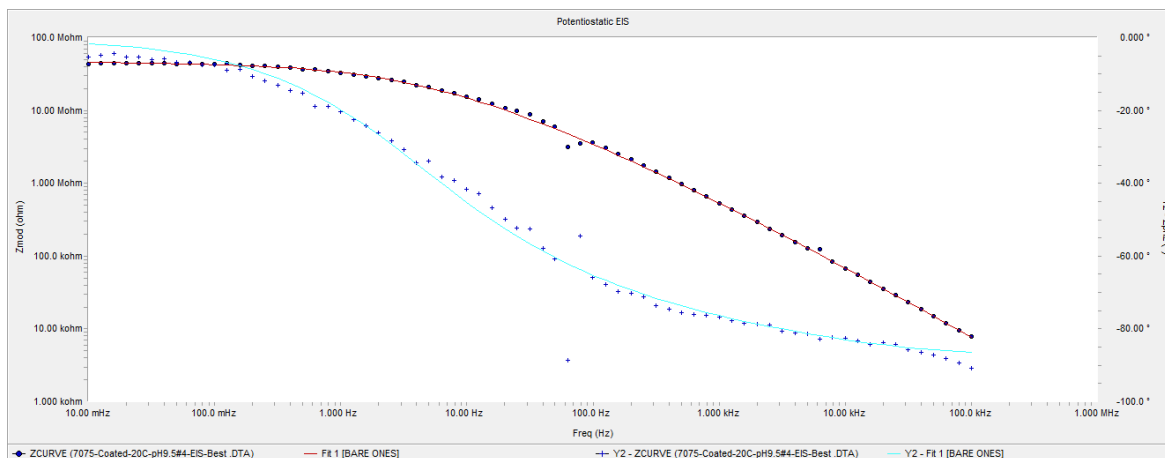
A 27. The bode plot diagram of a bare AA 7075-T6 sample at 40 °C and pH 9.5



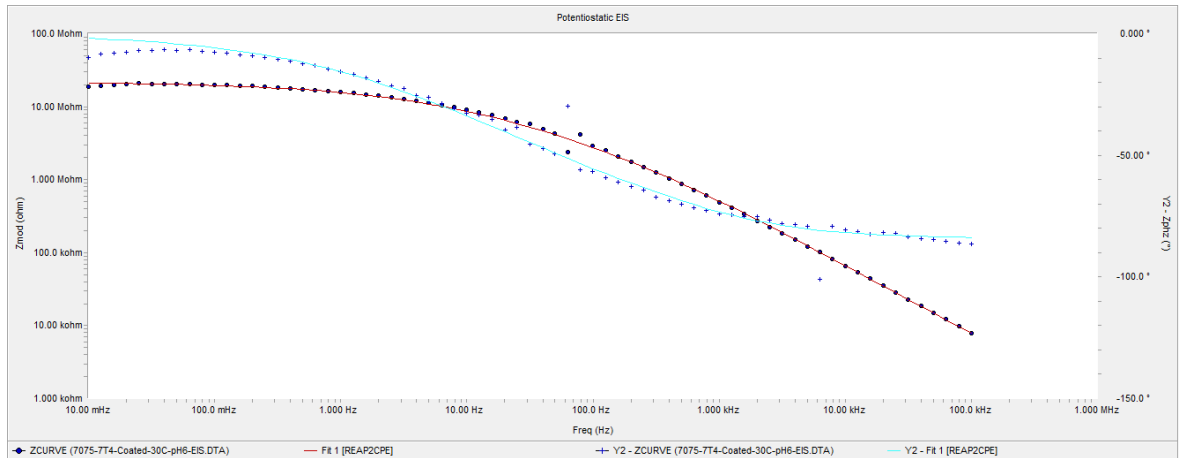
A 28. The bode plot diagram of a coated AA 7075-T6 sample at 20 °C and pH 6



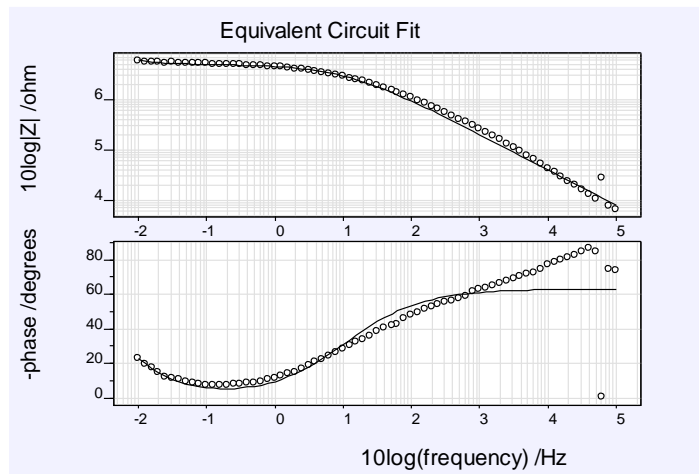
A 29. The bode plot diagram of a coated AA 7075-T6 sample at 20 °C and pH 7.9



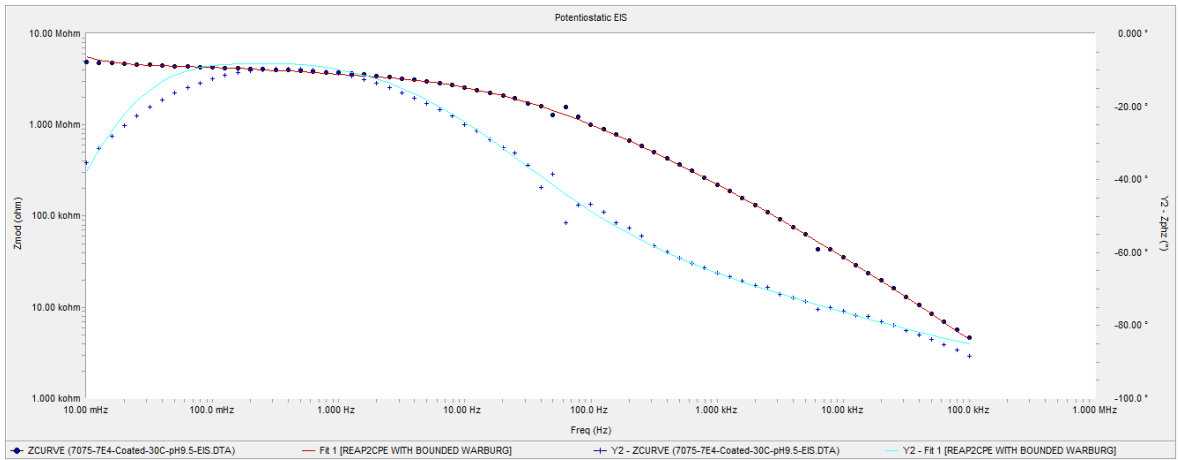
A 30. The bode plot diagram of a coated AA 7075-T6 sample at 20 °C and pH 9.5



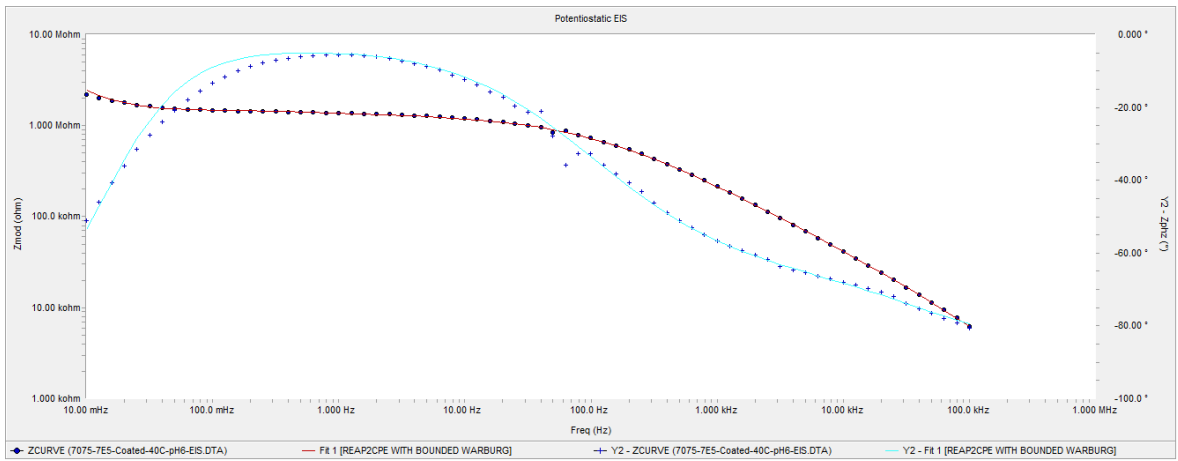
A 31. The bode plot diagram of a coated AA 7075-T6 sample at 30 °C and pH 6



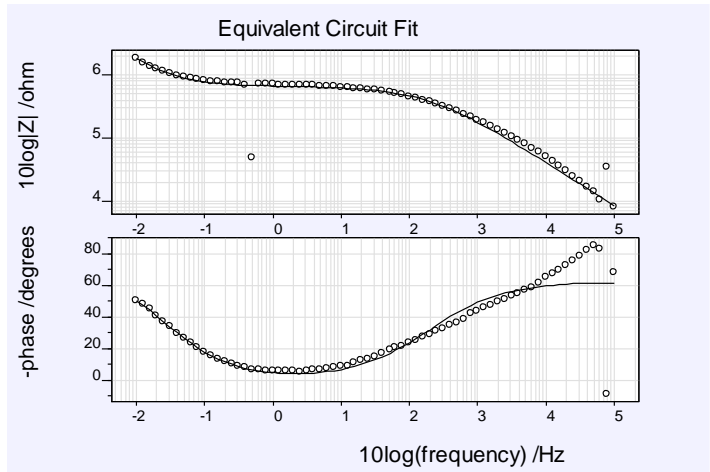
A 32. The bode plot diagram of a coated AA 7075-T6 sample at 30 °C and pH 7.9



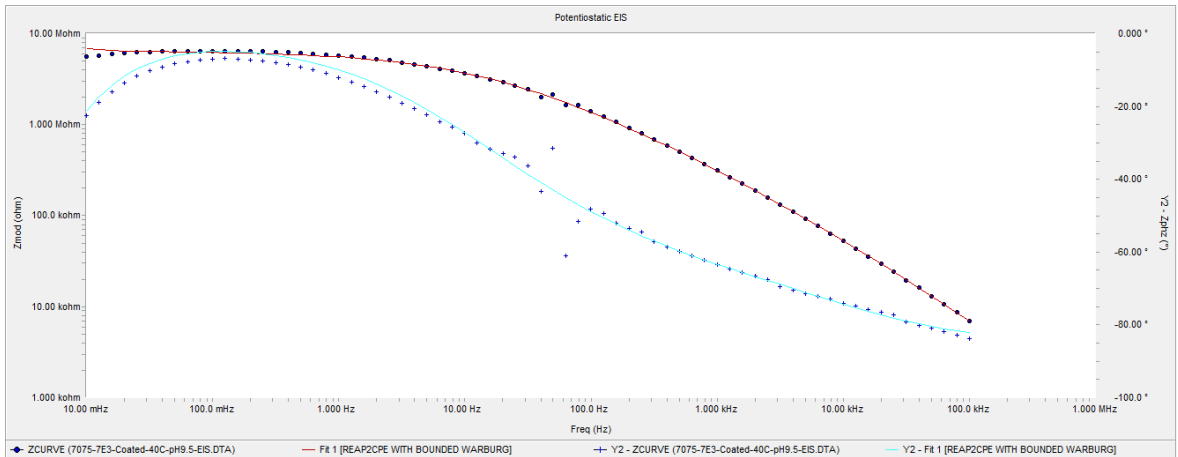
A 33. The bode plot diagram of a coated AA 7075-T6 sample at 30 °C and pH 9.5



A 34. The bode plot diagram of a coated AA 7075-T6 sample at 40 °C and pH 6



A 35. The bode plot diagram of a coated AA 7075-T6 sample at 40 °C and pH 7.9



A 36. The bode plot diagram of a coated AA 7075-T6 sample at 40 °C and pH 9.5

References

- [1] <http://navyaviation.tpub.com/14014/css/Chapter-4-Aircraft-Basic-Construction-73.htm>
- [2] Immarigeon, J. P., et al. "Lightweight materials for aircraft applications." *Materials characterization* 35.1 (1995): 41-67.
- [3] <https://www.azom.com/article.aspx?ArticleID=12117>
- [4] Mouritz, Adrian P. *Introduction to aerospace materials*. Elsevier, 2012.
- [5] Davis, Joseph R. "Aluminum and aluminum alloys." (2013).
- [6] Perryman, Jon. "Corrosion resistance of aluminum." A CMI Technical White Paper, Crane Materials International, Atlanta, GA (2007).
- [7] Ezuber, Hosni, A. El-Houd, and F. El-Shawesh. "A study on the corrosion behavior of aluminum alloys in seawater." *Materials & Design* 29.4 (2008): 801-805.
- [8] E. H. Dix, "'Alclad' a New Corrosion Resistant Aluminum Product," National Advisory Committee for Aeronautics, Washington, 1927.
- [9] G. M. Scamans, N. Birbilis and R. G. Buchheit, "Corrosion of aluminum and its alloys," in *Shreir's Corrosion*, vol. 3, *Corrosion and Degradation of Engineering Materials*, Amsterdam, Elsevier, 2010, pp. 1974-2010
- [10] Farrier, Lisa M., and Stephen L. Szaruga. "Sample preparation and characterization of artificially aged aircraft coatings for microstructural analysis." *Materials characterization* 55.3 (2005): 179-189.

- [11] Twite, R. L., and G. P. Bierwagen. "Review of alternatives to chromate for corrosion protection of aluminum aerospace alloys." *Progress in organic coatings* 33.2 (1998): 91-100.
- [12] A. A. Adjorlolo and J. A. Marceau, "Commercial aircraft," in *Corrosion Test and Standards: Application and Interpretation*, West Conshohocken, ASTM International, 2005, pp. 687-692.
- [13] N. Birbilis and B. Hinton, "Corrosion and corrosion protection of aluminium," in *Fundamentals of Aluminium Metallurgy: Production, Processing and Applications*, Cambridge, UK ; Philadelphia, Woodhead Publishing Ltd., 2011, pp. 574-604.
- [14] <https://www.corrosionclinic.com>. (2018). [Online] Available at: https://www.corrosionclinic.com/types_of_corrosion/crevice_corrosion.htm [Accessed Oct. 2018].
- [15] <https://www.substech.com> (2018). [online] Available at: https://www.substech.com/dokuwiki/doku.php?id=crevice_corrosion [Accessed 21 Oct. 2018].
- [16] Bautista, A. "Filiform corrosion in polymer-coated metals." *Progress in Organic Coatings* 28.1 (1996): 49-58.
- [17] Leidheiser Jr, Henry. "Corrosion of painted metals—a review." *Corrosion* 38.7 (1982): 374-383.
- [18] Theiler, F. P. "Corrosion Behavior of Aluminum." *Oxit* 3 (1989): 9-14.
- [19] Le Bozec, N., et al. "Investigation of filiform corrosion on coated aluminum alloys by ftir microspectroscopy and scanning kelvin probe." *Journal of the Electrochemical Society* 149.9 (2002): B403-B408.
- [20] <https://www.substech.com> (2018). [online] Available at: https://www.substech.com/dokuwiki/doku.php?id=intergranular_corrosion [Accessed 21 Oct. 2018].

- [21] <https://www.nace.org>. (2018). [online] Available at: <https://www.nace.org/Corrosion-Central/Corrosion-101> [Accessed 21 Oct. 2018].
- [22] C. Vargel, Corrosion of Aluminum, Burlington: Elsevier Science, 2004.
- [23] E. Ghali, Corrosion Resistance of Aluminum and Magnesium Alloys Understanding, Performance, and Testing, Hoboken: John Wiley & Sons, Inc., 2010.
- [24] P. K. Rout, M. M. Ghosh and K. S. Ghosh, "Influence of aging treatments on alterations of microstructural features and stress corrosion cracking behavior of an Al-Zn-Mg alloy," Journal of Materials Engineering and Performance, vol. 24, no. 7, 2015, pp. 2792-2805.
- [25] J. R. Davis, Corrosion of aluminum and aluminum alloys, Materials Park: ASM International, 1999
- [26] Hughes, Anthony E., et al. "High strength Al-alloys: microstructure, corrosion and principles of protection." Recent Trends in Processing and Degradation of Aluminium Alloys. InTech, 2011.
- [27] <http://www.sweethaven02.com.com>. (2018). [Online] Available at: http://www.sweethaven02.com/Aviation/MaintHandbook/ama_Ch08.pdf [Accessed Oct. 2018].
- [28] Kendig, M. W., A. J. Davenport, and H. S. Isaacs. "The mechanism of corrosion inhibition by chromate conversion coatings from X-ray absorption near edge spectroscopy (XANES)." Corrosion Science 34.1 (1993): 41-49.
- [29] Seon, F. M. "Rare earths for materials corrosion protection." Journal of the Less Common Metals 148.1-2 (1989): 73-78.
- [30] Breslin, C. B., G. Treacy, and W. M. Carroll. "Studies on the passivation of aluminium in chromate and molybdate solutions." Corrosion science 36.7 (1994): 1143-1154.

- [31] B.N. McBane, *Aulomotive Coatings*, Federation of Societies for Coatings Technology, Philidelphia, PA, 1987, p. 12.
- [32] MacQueen, R. C., R. R. Miron, and R. D. Granata. "Method for corrosion inhibitor mechanism studies in epoxy coated aluminium." *JCT, Journal of coatings technology* 68.857 (1996): 75-82.
- [33] Shi, Hongwei, et al. "Protection of 2024-T3 aluminum alloy by corrosion resistant phytic acid conversion coating." *Applied Surface Science* 280 (2013): 325-331.
- [34] Shi, Hongwei, En-Hou Han, and Fuchun Liu. "Corrosion protection of aluminum alloy 2024-T3 in 0.05 M NaCl by cerium cinnamate." *corrosion science* 53.7 (2011): 2374-2384.
- [35] Rodriguez, David, Roshan Misra, and Dev Chidambaram. "Molybdate-Based Conversion Coatings for Aluminum Alloys Part I: Coating Formation." *ECS Transactions* 45.28 (2013): 1-12.
- [36] Iribarren-Mateos, José Ignacio, et al. "Silane and epoxy coatings: A bilayer system to protect AA2024 alloy." *Progress in Organic Coatings* 81 (2015): 47-57.
- [37] Zhu, Wen, et al. "Comparative study on Ti/Zr/V and chromate conversion treated aluminum alloys: Anti-corrosion performance and epoxy coating adhesion properties." *Applied Surface Science* 405 (2017): 157-168.
- [38] Li, Liangliang, Brandon W. Whitman, and Greg M. Swain. "Characterization and performance of a Zr/Ti pretreatment conversion coating on AA2024-T3." *Journal of The Electrochemical Society* 162.6 (2015): C279-C284.
- [39] Liang, Chang-Sheng, et al. "Protection of aluminium foil AA8021 by molybdate-based conversion coatings." *Applied Surface Science* 288 (2014): 497-502.
- [40] Loveday, David, Pete Peterson, and Bob Rodgers. "Evaluation of organic coatings with electrochemical impedance spectroscopy" *JCT coatings tech* 8 (2004): 46-52.

[41] Y. Zheng, B. Brown, and S. Netic, "Electrochemical study and modeling of H₂S corrosion of mild steel," CORROSION/2013, NACE Int., Paper no. 2406, pp. 1–22, 2013.